AD-A073 425 ADVANCED ENGINEERING LAB ADELAIDE (AUSTRALIA) F/G 20/1
AN INTRODUCTION TO THE DESIGN OF SURFACE ACOUSTIC WAVE DEVICES.(U)
APR 78 R DOBSON

UNCLASSIFIED AEL-0001-TR

| OF |
AD A073425

END
DATE FILMED
10-79
DDC

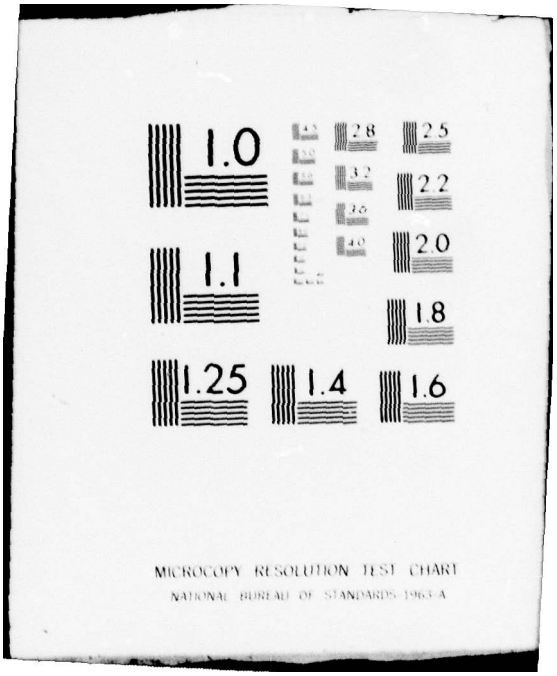
1.0
1.1
1.25
1.4
1.6
2.8
3.2
3.6
4.0
2.5
2.2
2.0
1.8
MICROCOPY RESOLUTION TEST CHART
NATIONAL BUREAU OF STANDARDS-1963-A

AEL-0001-TR

LEVEL II

12

B.S.

AR-001-177

DEPARTMENT OF DEFENCE

DEFENCE SCIENCE AND TECHNOLOGY ORGANISATION

ADVANCED ENGINEERING LABORATORY

DEFENCE RESEARCH CENTRE SALISBURY
SOUTH AUSTRALIA

TECHNICAL REPORT

AEL-0001-TR

AN INTRODUCTION TO THE DESIGN OF SURFACE ACOUSTIC WAVE DEVICES

R. DOBSON

Approved for Public Release.

COPY No. 19

AR-001-177

DEPARTMENT OF DEFENCE

DEFENCE SCIENCE AND TECHNOLOGY ORGANISATION

ADVANCED ENGINEERING LABORATORY

(9) TECHNICAL REPORT

(14) AEL-0001-TR

(6) AN INTRODUCTION TO THE DESIGN OF SURFACE ACOUSTIC WAVE DEVICES

(10) R. Dobson

(11) Apr 78

(12) 68 p.

SUMMARY

Surface acoustic wave devices such as bandpass filters, matched filters and oscillators are in general one or two orders of magnitude smaller than their conventional electromagnetic counterparts and in many applications provide superior performance. This note provides a brief introduction to the fundamental properties of surface acoustic waves and some of the more common surface acoustic wave devices. The practical considerations for surface acoustic wave device design are discussed and some results are given.

Approved for Public Release

POSTAL ADDRESS: Chief Superintendent, Advanced Engineering Laboratory, Box 2151, G.P.O., Adelaide, South Australia, 5001.

DOCUMENT CONTROL DATA SHEET

Security classification of this page: UNCLASSIFIED

1 DOCUMENT NUMBERS	
AR Number:	AR-001-177
Report Number:	AEL-0001-TR
Other Numbers:	

2 SECURITY CLASSIFICATION	
a. Complete Document:	UNCLASSIFIED
b. Title in Isolation:	UNCLASSIFIED
c. Summary in Isolation:	UNCLASSIFIED

3 TITLE

AN INTRODUCTION TO THE DESIGN OF SURFACE ACOUSTIC WAVE DEVICES

4 PERSONAL AUTHOR(S):

R. Dobson

5 DOCUMENT DATE: April 1978

6 6.1 TOTAL NUMBER OF PAGES: 67

6.2 NUMBER OF REFERENCES: 69

7 7.1 CORPORATE AUTHOR(S):

Defence Research Centre Salisbury
Advanced Engineering Laboratory

7.2 DOCUMENT SERIES AND NUMBER
Advanced Engineering Laboratory
0001-TR

8 REFERENCE NUMBERS

a. Task:

b. Sponsoring Agency:

9 COST CODE: 048008

10 IMPRINT (Publishing organisation)

Defence Research Centre Salisbury

11 COMPUTER PROGRAM(S) (Title(s) and language(s))

12 RELEASE LIMITATIONS (of the document):

Approved for Public Release

12.0	OVERSEAS	NO		P.R.	1	A		B		C		D		E	

Security classification of this page: UNCLASSIFIED

Security classification of this page: UNCLASSIFIED

13 ANNOUNCEMENT LIMITATIONS (of the information on these pages):

No limitation.

14 DESCRIPTORS:		15 COSATI CODES:
a. EJC Thesaurus Terms	Acoustic signals Elastic waves Acoustics Acoustic filters Bandpass filters Surface waves Acoustic measurement transducers	2001 1402
b. Non-Thesaurus Terms	Surface acoustic waves	

16 LIBRARY LOCATION CODES (for libraries listed in the distribution):

SW SR SD AACA

17 SUMMARY OR ABSTRACT:
(if this is security classified, the announcement of this report will be similarly classified)

Surface acoustic wave devices such as bandpass filters, matched filters and oscillators are in general one or two orders of magnitude smaller than their conventional electromagnetic counterparts and in many applications provide superior performance. This note provides a brief introduction to the fundamental properties of surface acoustic waves and some of the more common surface acoustic wave devices. The practical considerations for surface acoustic wave device design are discussed and some results are given.

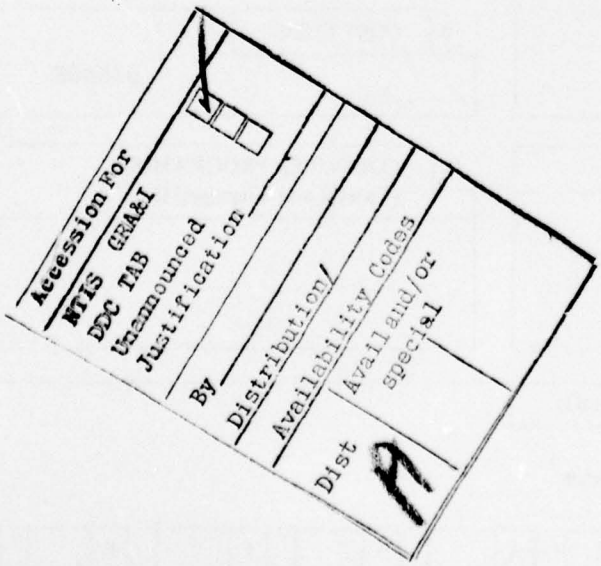

Security classification of this page: UNCLASSIFIED

TABLE OF CONTENTS

LIST OF TABLES

LIST OF FIGURES

Page No.

1. INTRODUCTION

Although Surface Acoustic Waves (SAW) were first studied by Lord Rayleigh in 1885, little interest had been shown in them until recently, except by those studying flaw detection in materials and those studying the geophysical consequences of earth tremors. SAW have been generated artificially for many years now by conversion of energy from bulk elastic waves; this method is relatively complicated, of low efficiency and is of little practical use. The great upsurge of interest in SAW came after 1965 when White and Voltmer[6]* announced the development of the interdigital transducer. This transducer is a metallised interdigital structure which is fabricated directly onto the surface of a piezoelectric substrate and interacts directly with the surface wave. As the interdigital transducer may be placed anywhere along the surface wave path, the device may be used as a tapped delay line. This coupled with the fact that the wave velocity is about 1/100,000 of the velocity of free electro-magnetic waves meant that SAW technology offered great potential for the development of novel devices and the miniaturization of conventional devices. Early device development, however, was plagued by "second order" effects which considerably reduced device performance and usefulness. Research over the past decade has enabled designers to reduce most of these "second order" effects to a level where many SAW devices now outperform conventional devices in many respects.

The maturing of SAW technology over this period has attracted an increasing number of potential SAW users and device designers. This report is intended to give a brief but broad overview of the subject; starting with the fundamental properties of surface waves, followed by a few of the more common SAW devices, with the bulk of the report being devoted to the practical design considerations and the elimination of "second order" effects. A sectionalised reference is included from which more detailed information may be obtained.

2. SURFACE ACOUSTIC WAVES

A detailed coverage of the theory and properties of electro-acoustic surface waves is given in [5], and only a brief treatment of surface acoustic or Rayleigh waves will be given here, from the device designers viewpoint.

2.1 Physical properties

Surface acoustic waves are elastic waves which propagate along the stress free surface of a body. Figure 1 shows a few cycles of a surface wave travelling down the surface of a piezo-electric substrate, the wave plot being obtained by means of an electrostatic probe.

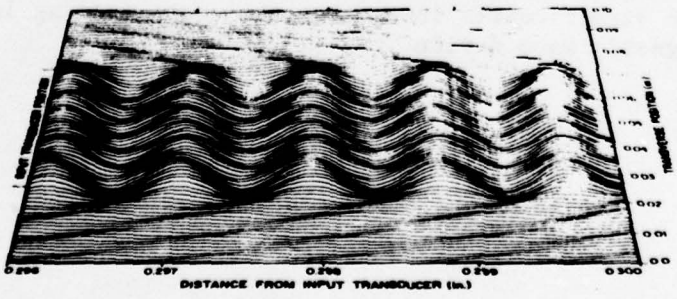

Figure 1. Surface acoustic waves

*[] Indicates a reference in the sectionalised reference. Note that not all entries in the reference are referred to in this report.

Typical particle displacement, illustrated in figure 2, results in two component strains, shear and compressional; the largest of these, the shear component, is normal to the propagating surface whilst the compressional component is parallel to the propagating surface and to the propagation direction. The particle motion is retrograde elliptical and the majority of the wave energy lies within one acoustic wavelength of the surface, this is also illustrated in figure 2. Figure 3 is a plot of the

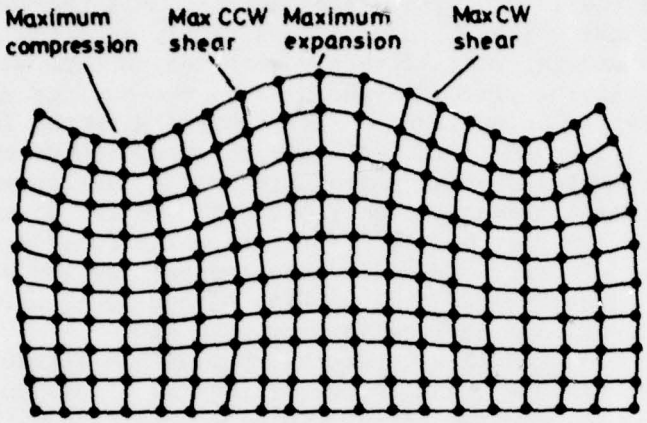

Figure 2. SAW particle displacement

magnitude of each component as a function of depth in wavelengths; note that the shear component is shifted one quarter wavelength along the wave normal from the compressional component to illustrate the quadrature relationship between these two. As the particles on the surface of a substrate are less constrained than those in the body of the substrate the velocity of a wave on a surface is less than the velocity of a bulk wave; thus the surface wave energy cannot propagate into the interior to become a bulk wave and it remains on the surface as a surface wave.

Surface acoustic waves have a wave velocity that is typically 3000 m/s or 1/100 000 of the velocity of electromagnetic waves, velocity being independent of frequency through the low microwave range. This means that devices implemented with surface wave delay lines will be correspondingly smaller than the same devices implemented with electromagnetic delay lines. Another significant feature of surface acoustic waves is that for a given time delay the propagation losses of a surface wave device are significantly lower than the corresponding losses of a guided electromagnetic wave device.

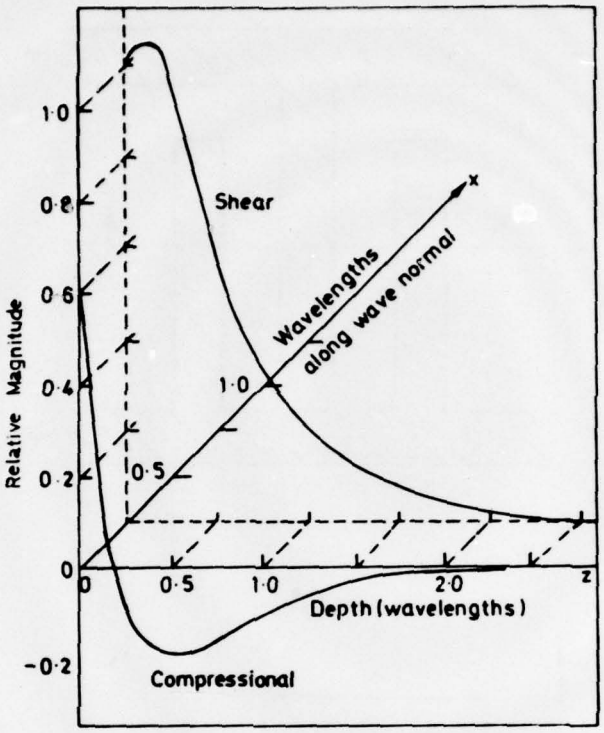

Figure 3. SAW shear and compressional components

2.2 The interdigital transducer

If metal electrodes are placed on the surface of a piezo-electric substrate as shown in figure 4 and a potential difference is applied between adjacent electrodes then an electric field will be set up as indicated. Note that this electric field may be broken into two orthogonal components which will, due to the inverse piezo-electric effect, create a mechanical stress with two orthogonal components. The stresses set up resemble those of a surface acoustic Rayleigh wave, thus if an impulse of electrical energy is applied between adjacent fingers then a standing wave will be set up on the piezo-electric surface which will then break up into its two components, launching a surface wave in each direction. The periodicity of this surface wave will be equal to the periodicity of the applied electric field or, the frequency of the wave will be the velocity of the surface wave divided by the interdigital finger pair spacing.

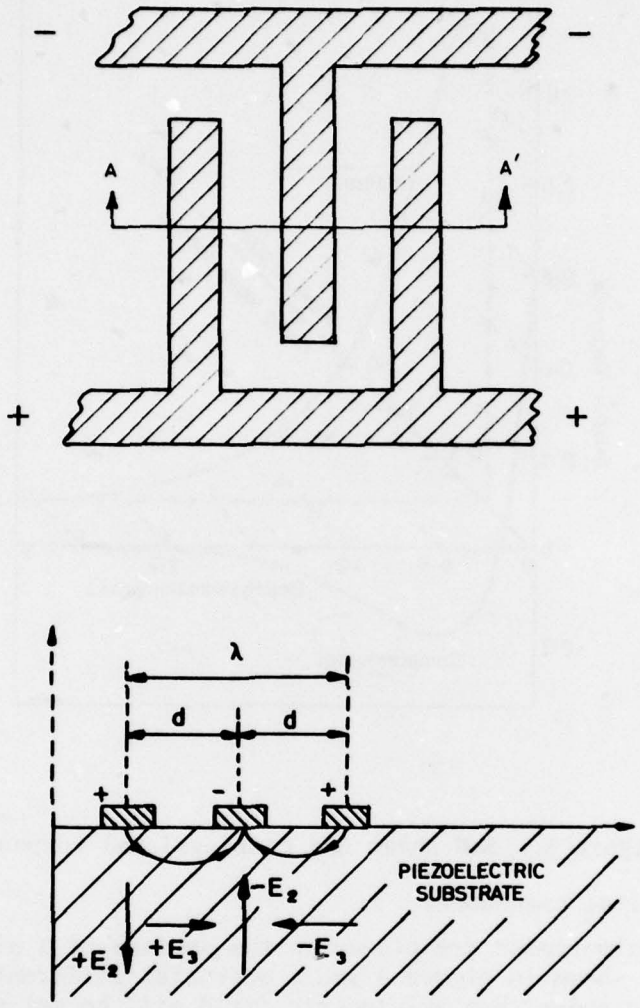

Figure 4. Interdigital transducer showing electric field components

Consider now figure 5, where the transducer on the left is launching a surface wave in the manner just described. As the wave propagating along the surface causes mechanical stress in the piezo-electric substrate, then there will be an electric field accompanying the mechanical stress due to the piezo-electric effect. This electric field may be "tapped off" anywhere along its propagation path by another interdigital transducer. Thus the interdigital transducer may be used to both launch and receive surface acoustic waves.

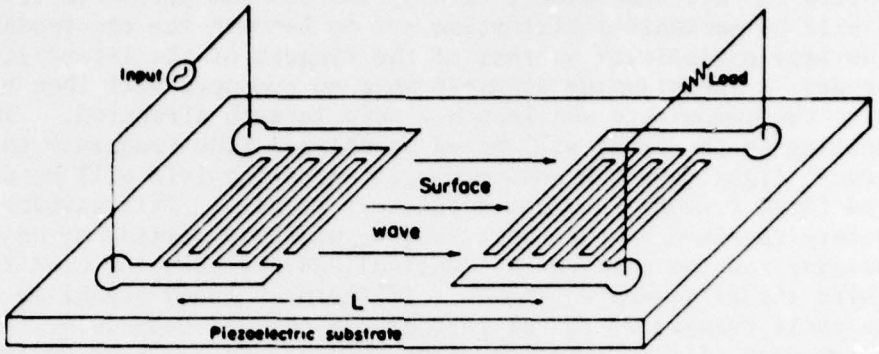

Figure 5. Interdigital launch and receive transducers

Each cycle generated by the launch transducer is as wide as the overlap of the finger pair that generates it. Consider now a cycle of sine wave of half the width of the launch transducer shown in figure 5 propagating under the receive transducer, the receiver transducer finger pairs integrate over their whole overlap width and so the sine wave of half width will appear across these electrodes as an electrical sine wave of half the amplitude of that of a full width wave. Thus the amplitude contribution of individual taps in a transducer may be controlled by varying the finger overlap - this is known as apodization.

As distance along the surface corresponds to time, then the phase of a signal may be varied by varying the position of the transducers. Thus the interdigital transducer allows precise control of frequency, phase and amplitude of signals on a surface wave delay line, or equivalently there is a unique correspondence between the metallization pattern of the transducers and the device's response to an impulse of electrical energy.

Interdigital transducers for the frequency range up to several hundred megahertz may be produced using standard photolithographic processing techniques used in the production of microelectronic circuits. Transducers covering the range up to low microwave frequencies may be manufactured by a more elaborate process using electron beam etching and laser interferometer positioning techniques.

3. SURFACE ACOUSTIC WAVE DEVICES

The principles of operation of a few of the more common surface wave devices will be discussed.

3.1 Chirp matched filter

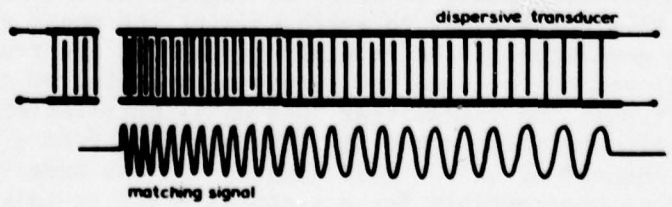

Figure 6. Chirp matched filter

Figure 6 shows an interdigital transducer which has its electrode spacing linearly increasing from left to right. If an electrical impulse is applied to this transducer, then by the inverse piezo-electric effect there will be mechanical distortion set up beneath the electrodes which has the same periodicity as that of the fingers of the interdigital electrodes. The standing acoustic wave so produced will then break up into its two components and launch a wave in each direction. The wave propagating to the right will be an up-chirped (low frequency to high frequency) signal and the wave propagating to the left will be a down-chirped (high frequency to low frequency) signal. This waveform is adequately received by the short length, wideband transducer on the left.

Consider now the case of an identical SAW device being used to receive the chirp signal generated above. If the up-chirped signal is applied to the small transducer to the left of the chirped transducer then the chirp waveform will be launched along the surface and pass under the chirped transducer. Very little response will be produced when the surface wave has different periodicity to the periodicity of the transducer taps and only at one point will be periodicity of each cycle in the train correspond to the periodicity of the tapping electrodes, at this point there will be a great increase in the output response. Thus the chirped transducer may be used for generating a chirped waveform and also as a matched filter for correlating this waveform.

3.2 Phase coded sequence generator/correlator

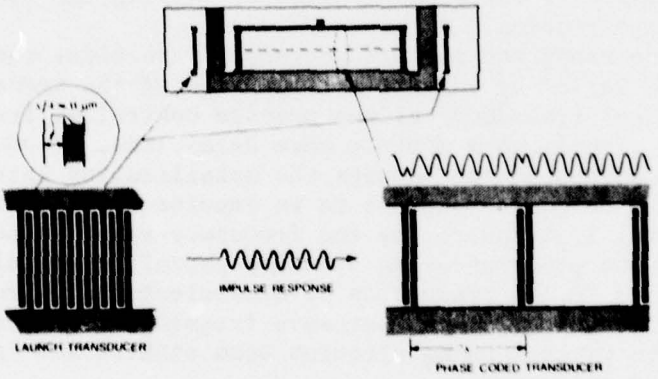

Figure 7. SAW phase coded sequence generation/correlator

In spread spectrum communications an information bearing carrier is phase reversed by a pseudo-random binary bit stream before transmission, this spreads the signal over a bandwidth many times greater than the information bandwidth and produces a low 'probability of intercept' signal with considerable anti-jam capability. At the receiver this phase-reversed carrier must be rephase-reversed in exactly the same points that the original phase reversals took place in order to regain the information from the carrier. This corresponds to synchronizing the phase reversing pseudo-random code generator in the receiver to that in the transmitter. The conventional method for code synchronization is to let the receiver code slowly drift past the transmitter code until correlation is achieved. Synchronization by this method may take anything from a few minutes to tens of minutes, depending on the code length, and has made spread spectrum communications unacceptable for a tactical press-to-talk applications.

It will now be shown how a surface acoustic wave correlator may be used to overcome these shortcomings. Consider the case of code generation. In figure 7 the transducers at either end of the substrate consist of N finger pairs with a periodicity corresponding to the desired RF carrier. If the transducer on the left has an electrical impulse applied to it then a train of N cycles of sine wave will be set up which will then propagate under the centre phase coded transducer. As these N cycles pass under each tap of the centre transducer then N cycles of sine wave will appear at the output, the phase of which will be determined by the phase coding of each tap. As the last cycle of sine wave finishes passing under one tap, the first cycle will start passing under the next tap and so a continuous stream of phase coded sine wave at the RF carrier will be produced until the wave train passes under the last tap.

A device identical to that used for generating the phase coded sequence may be used to correlate the sequence. Consider the phase coded sequence generated above being applied to the transducer on the right of figure 7. This sequence will propagate under the phase coded taps and at one point only will the phase coding of the sequence correspond to the phase coding of the taps and produce a correlation peak; at all other times the contributions of the phase coded taps will tend to cancel each other out. The amplitude of the correlation peak is proportional to the number of taps.

3.3 SAW bandpass filters

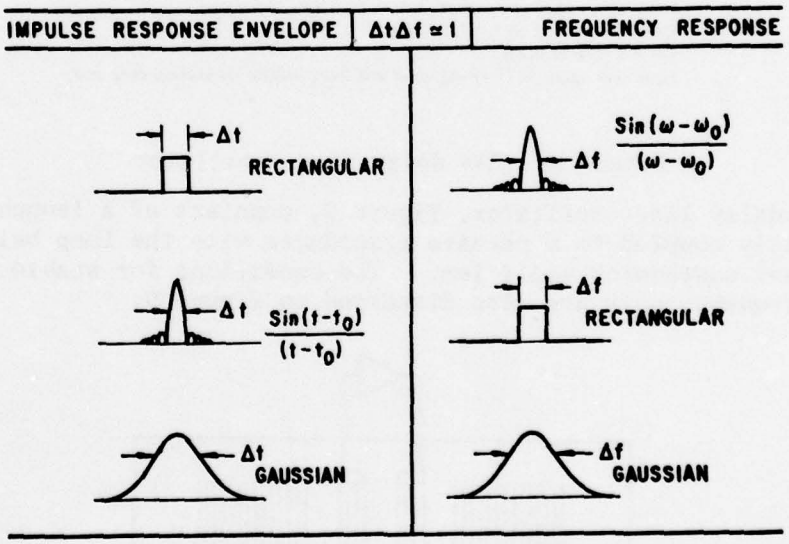

Figure 8. Bandpass filters and their impulse responses

3.4 SAW oscillators

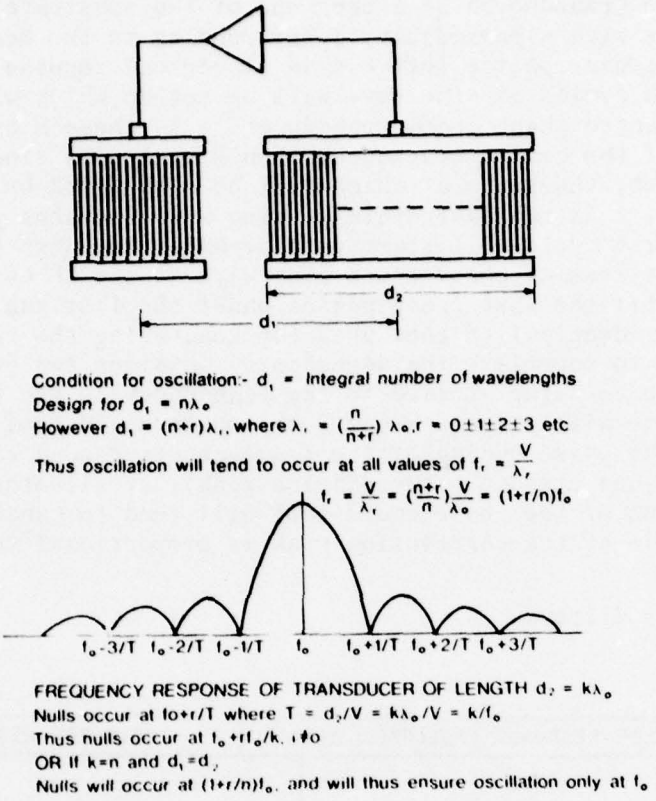

Figure 9. SAW delay line oscillator

A SAW delay line oscillator, figure 9, consists of a launch transducer acoustically coupled to a receive transducer with the loop being closed by an external sustaining amplifier. The conditions for stable oscillation at one frequency only are also discussed on figure 9.

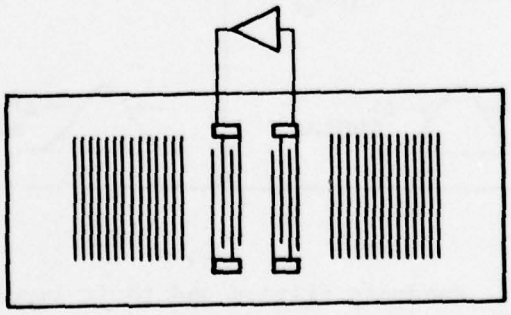

Figure 10. SAW resonator oscillator

Another type of SAW oscillator which has been developed more recently is the resonator controlled oscillator shown in figure 10. This oscillator relies on reflections from periodic discontinuities placed at half wavelength spacings to create a resonant structure.

SAW oscillators using ST cut quartz substrates have a stability which is considerably better than the common inductor-capacitor (LC) oscillator, but is not as good as the crystal controlled oscillator. SAW oscillators do not rely on harmonic operation as do some crystal oscillators and,

with current technology, may be fabricated for fundamental operation in the low microwave range. The volume of a SAW oscillator may be an order less than the equivalent LC oscillator.

3.5 SAW frequency synthesisers

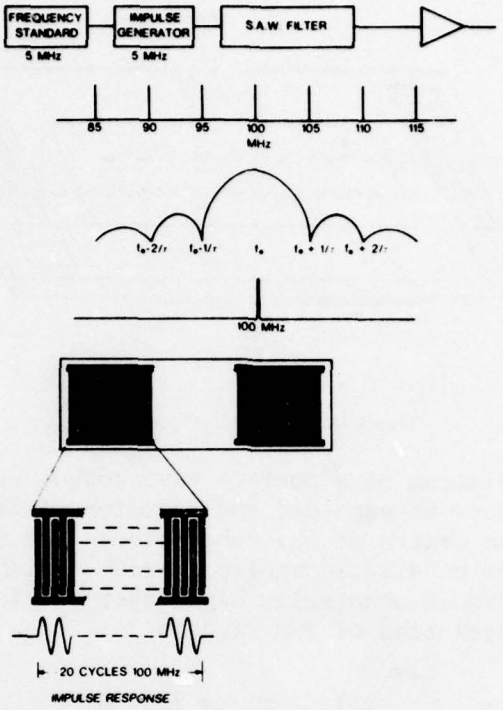

Figure 11. SAW frequency synthesiser

The details of a SAW frequency synthesiser are shown in figure 11. An impulse generator is used to generate the harmonics of a stable frequency source, and a SAW filter is used to filter out the desired harmonic. If the SAW filter is constructed so that all the fingers are of uniform overlap (unapodized) then the resulting frequency response will be the familiar sin x/x pattern. By selecting the appropriate number of fingers in the interdigital transducer, the nulls in the sin x/x pattern can be made to have the same spacing as the harmonics of the frequency source and so all of the undesired harmonics can be rejected. The thought of having 20 filters to synthesise 20 different frequencies sounds bulky and expensive by conventional standards, however, SAW filters are very small with 10 filters/cm^2 not being uncommon for the above application, and in fact a SAW frequency synthesiser may be one or two orders of magnitude smaller than a conventional frequency synthesiser.

SAW synthesisers are ideally suited to communication systems where a number of channels are separated by a fixed frequency difference.

3.6 SAW convolvers

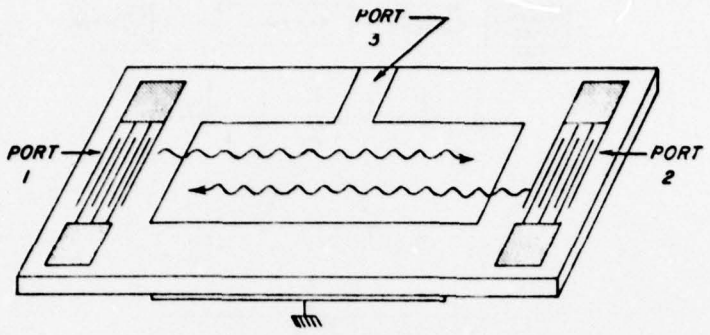

Figure 12. SAW convolver

A schematic diagram of a surface wave convolver is shown in figure 12. It has a transducer at each end and detector electrode plates on the top and bottom in the centre of the substrate. The SAW convolver is unusual in that it relies on elastic nonlinearities, which become evident when the device is operated at abnormally high power levels, to generate product terms. The convolution of two signals

$$f(t) * g(t) = \int_{-\infty}^{+\infty} f(t - \tau)\ g(\tau)\ d\tau$$

may be thought of as the integration of the product of g (τ) and a time reversed f (t) as they are slid past each other. The same process may be seen to occur on the surface wave convolver of figure 12. Consider an RF carrier (ω_1) modulated by f (t) being launched from port 1 and the same carrier modulated by g (t) being launched from port 2. As these contradirectional waves pass each other the nonlinearities of the device gives rise to a product term which is then integrated by the large detector plates of port 3. This output (at ω_1) is the convolution of f (t) and g (t) time compressed by a factor of two. If the duration of f (t) and g (t) is less than the transit time under the pick up plate, then the integration limits may be taken to be infinite. The convolver of figure 12 is a special case in that f (t) and g (t) modulate the same carrier frequency, this is known as a degenerate convolver. Convolvers in which f (t) and g (t) modulate different frequency carriers have the detector plate replaced by an interdigital array which operates at the difference of the carrier frequencies. SAW convolvers using simple piezoelectric substrates to generate non-linear effects are relatively inefficient and most practical convolvers are semiconductor coupled and rely on the nonlinearities in the semiconductor.

SAW convolvers may be used in a wide variety of applications including waveform correlation and the generation of real time Fourier Transforms of signals.

4. PRACTICAL CONSIDERATIONS

The ideal surface acoustic wave may be thought of as a parallel wave the width of the launching transducer travelling unattenuated down the length of the substrate, with the conversion of electrical energy to acoustic energy and back again being one hundred percent efficient. The deficiencies of practical devices will now be discussed.

4.1 Substrate attenuation

The attenuation of a surface acoustic wave due to the substrate material has been found to be approximately proportional to the square of the operating frequency [50]. Both magnitude and frequency dependence of the attenuation are important parameters to be considered when high percentage bandwidth filters are being designed. Curves of attenuation against frequency for Quartz, Lithium Niobate and Bismuth Germanium Oxide, the most common surface wave substrates, are illustrated in figure 13. Note that Quartz has more than twice the attenuation per given delay than has Lithium Niobate. (Both have delay times of approximately 3 μs/cm.) For devices designed to operate in the lower VHF region, the attenuation will be negligible except where very long time delays are being considered.

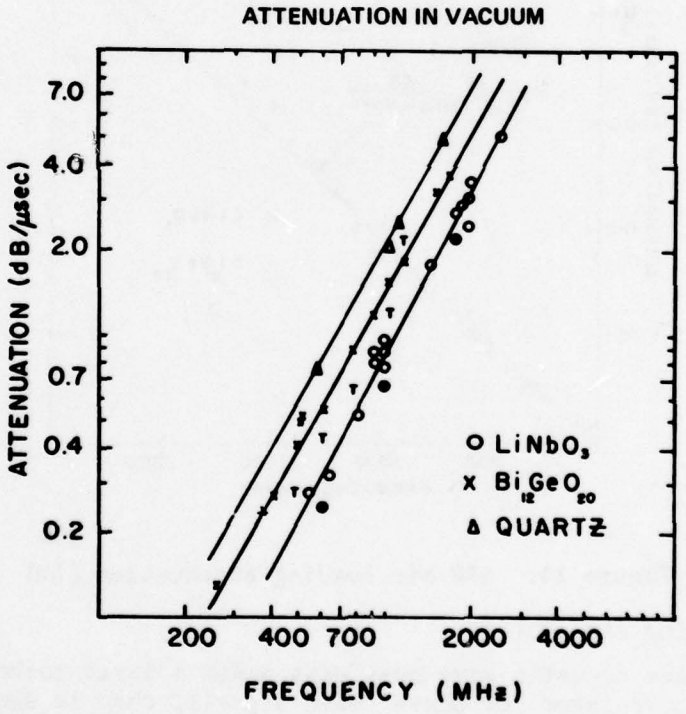

Figure 13. SAW substrate attenuation [50]

Empirical expressions for the substrate attenuation curves of figure 13 have been derived [50]:

Y cut, Z propagation $LiNbO_3$ loss (db/μs) = $0.88F^{1.9}$ ....(1)

001, 110, $Bi_{12}GeO_{20}$ loss (db/μs) = $1.45F^{1.9}$ ....(2)

Y cut, X propagation Quartz loss (db/μs) = $2.15F^{2}$ ....(3)

where F is the operating frequency in GH_z

4.2 Air loading attenuation

Curves of surface acoustic wave attenuation as a function of operating frequency are illustrated in figure 14 (from [50]) where it can be seen that attenuation is proportional to the operating frequency. Again the effects are negligible in the low VHF range, but should be considered in the UHF and microwave frequencies. Fortunately, air loading can be eliminated by vacuum encapsulation or by using a light gas (e.g. Helium) environment.

Empirical expressions for the air loading attenuation curves of figure 14 have been derived [50] :

Y cut, Z propagating $LiNbO_3$ loss (db/μs) = 0.19F ....(4)

001, 110, $BiGeO_{20}$ loss (db/μs) = 0.19F ....(5)

Y cut, X propagating Quartz loss (db/μs) = 0.45F ....(6)

where F is the operating frequency in GH_z

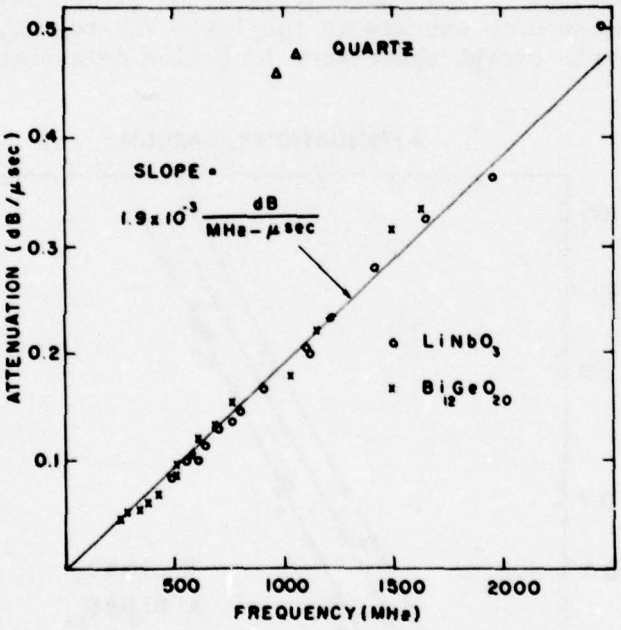

Figure 14. SAW air loading attenuation [50]

4.3 Energy coupling attenuation

If a surface acoustic wave must pass under a large number of taps, as occurs in a correlator for phase coded signals, then it should ideally remain unattenuated down the entire path length. To achieve this, the coupling coefficient of each of the taps must be kept very low, otherwise energy will be taken off at each tap along the path length, resulting in a severely attenuated signal for the final taps. The degree of signal attenuation due to this cause may be calculated from the power scattering parameters given in the section on transducer equivalent circuit models.

4.4 Transducer coupling losses

These losses are those associated with the launching and receiving of the surface wave. The most common type of interdigital transducer is bidirectional and launches waves in both forward and reverse directions, the reverse wave usually being absorbed by an acoustic absorbing material such as silastic or black vacuum wax. Bidirectionality results in a 3db loss in launching and another 3db loss in receiving due to reciprocity.

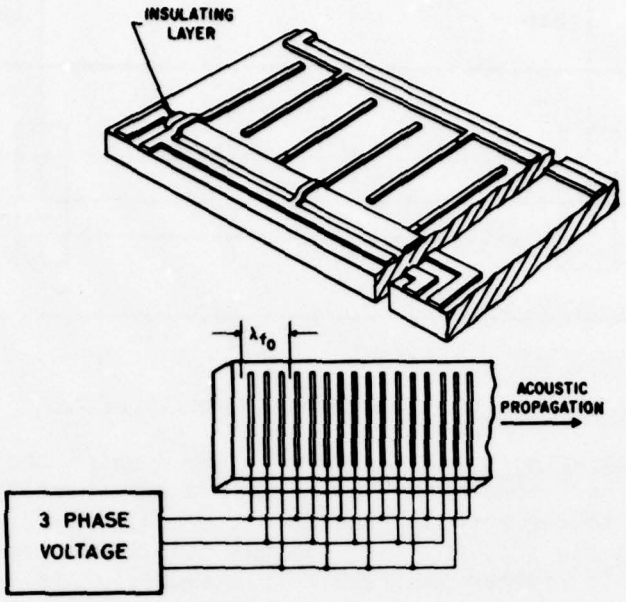

Figure 15. The unidirectional transducer

The unidirectional transducer (figure 15) overcomes these losses to a large extent and will be discussed in the section on transducer design. Further losses occur in the electrical matching network used to match the electrical source to the transducer. A typical value for this loss being about 4db overall. If a broadband response is required, then the electrical circuit Q must be damped appropriately, which will cause even further losses.

4.5 Electro-acoustic regeneration

As a surface acoustic wave propagates under a bidirectional transducer, an electric field appears between adjacent fingers due to the piezo-electric effect. This field is applied to all of the electrically connected fingers in the array which, in turn, causes a mechanical stress on the surface of the substrate due to the inverse piezo-electric effect which then becomes a new surface acoustic wave propagating bidirectionally from the transducer. This effect occurs in both the launch and receive transducers. The wave which is relaunched in the opposite direction to the incident wave is called the reflected wave.

Consider the case of a wave which is incident on an ideally terminated bidirectional receive transducer. Only one half of the incident wave energy will be absorbed, the other half will be relaunched bidirectionally (see figure 16).

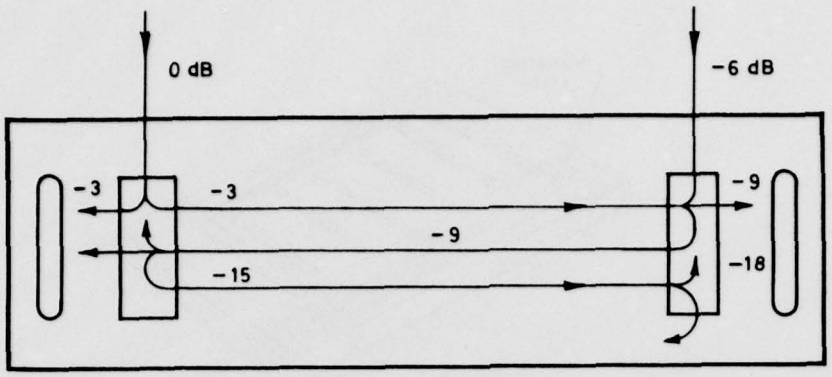

Figure 16. The triple transit effect

The reflected wave, which will now be 6db down on the incident wave, will propagate back toward the launch transducer where it will be reflected back to the receive transducer. This re-reflected wave will be 12db down on the incident wave and has done three transits down the substrate when it reaches the receive transducer. It is known as the triple transit wave and will produce a delayed spurious response 12db down on the main response.

Electro-acoustic regeneration can cause severe problems in transducers which have groups of taps spaced periodically as occurs in comb filters and phase coded transducers. In these cases, reflections occur between groups of taps, which causes stop bands to be generated at harmonics of the group spacing frequency (this corresponds to harmonics of the chip rate in a phase coded transducer). Judd et. al. [42], have shown that a successful method of removing these stop bands is to place dummy electrodes between the tap groups as in figure 17. The improvement in response by using dummy electrodes is shown in figure 18.

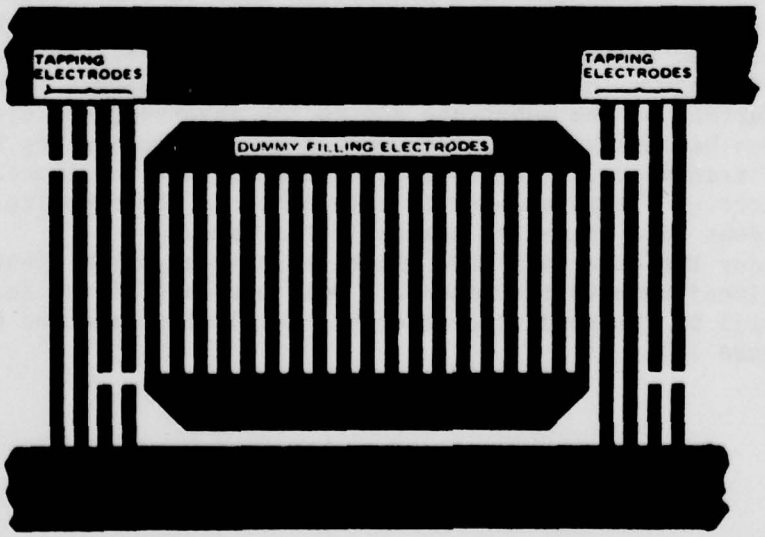

Figure 17. Dummy filling electrodes

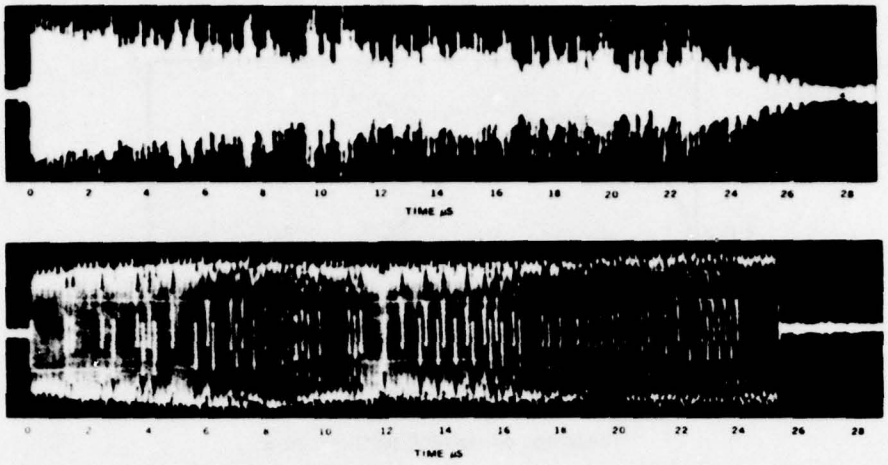

Figure 18. Impulse responses of a phase coded transducer without (top) and with (bottom) dummy filling electrodes [42]

Electro-acoustic regeneration and its associated problems may be virtually eliminated by careful design. Firstly, if a unidirectional transducer (figure 15) is used, most of the energy launched at one end will be received at the other end, providing the electrical network is correctly matched. To match the electrical network correctly, the capacitance of the interdigital transducer array must be made to resonate with an external inductor at the frequency of acoustic resonance of the surface wave transducer. To reduce reflections in the case of a bidirectional transducer, a damping resistor may be placed across the electrical matching network which virtually shorts out the piezo-electric field. This has the disadvantage of severely attenuating the received signal; however, in many cases this may be entirely acceptable. Transducer scattering parameters may be used to determine the level of reflections due to this cause for various load conditions.

4.6 Reflections due to presence of metal electrodes

4.6.1 Electro-acoustic impedance mismatch

Each interdigital electrode edge encountered by a surface wave represents a discontinuity in the propagating medium, this causes a fraction of the surface wave energy to be reflected which results in spurious responses. The presence of a conducting electrode on the surface of a piezo-electric propagating medium causes changes in both the electro-acoustic impedance and wave velocity. These parameters change because the electrodes short circuit the electric field, the effect being more severe in the substrates with high coupling coefficients. Note that reflections due to this cause are independent of load and are not related to electro-acoustic regeneration. Emtage [56], has carried out an analysis of interdigital transducers which includes reflections due to the electrode short circuiting effect, and concludes that reflections due to this cause become significant when $(4N\ S\ \Delta v/v_{oo})$ becomes of the order of unity. N is the number of finger pairs and the parameter S is a reflection coefficient, illustrated in figure 19, as a function of the fraction of substrate surface

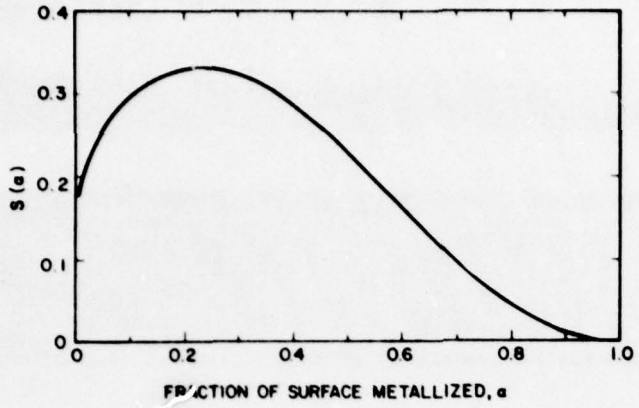

Figure 19. Short circuit reflection parameter 'S' [56]

metallised. The amplitude reflection and transmission coefficients for a short circuited single finger pair are given by:

$$\text{Reflection coefficient} = i \sin 2\pi S \left(\Delta v / v_\infty\right) \quad \ldots.(7)$$

$$\text{Transmission coefficient} = \cos 2\pi S \left(\Delta v / v_\infty\right) \quad \ldots.(8)$$

Reflections due to acoustic impedance mismatch may be reduced by increasing the fraction of surface metallised (reducing S) or may virtually be eliminated by use of split fingers [38] or a tilted transducer geometry [52]. The split finger geometry is shown in figure 20 where it can be seen that the finger spacing and width are both $\lambda/8$ instead of the usual $\lambda/4$, this causes the most efficient reflection frequency to be at twice the operating frequency which can be considered as being out of band for most applications.

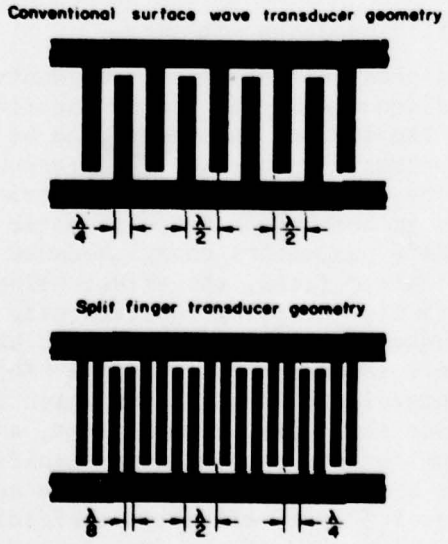

Figure 20. A comparison of conventional and split finger transducer geometry

Figure 21 (from [55]) presents a comparison of reflection coefficients at the fundamental for both conventional and split finger geometries. Note that the reflection coefficient of the split finger geometry is independent of the number of fingers. A disadvantage of the split finger geometry is that the upper frequency limit is halved for a given fabrication process, unless harmonic operation is utilised.

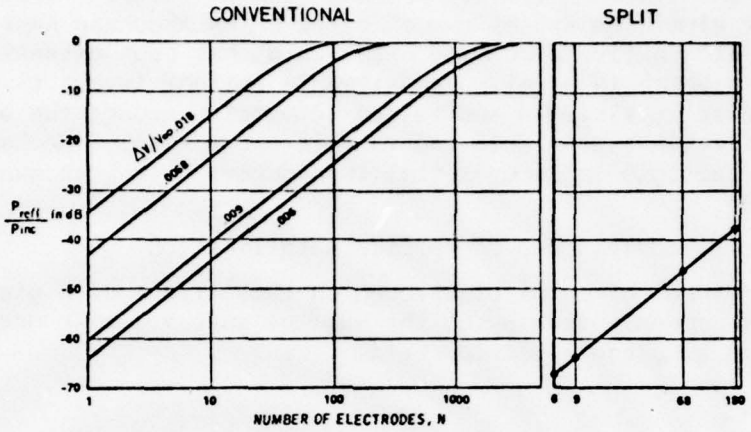

Figure 21. A comparison of reflections from convential and split fingered transducer geometries [55]

An alternative to the split finger geometry, the tilted transducer geometry, is shown in figure 22. A wave launched from one of the transducers passes under only a few of the fingers of the second transducer, thus reducing the reflections considerably. The effect of the wave travelling under the busbar appears to be negligible. The disadvantage of the tilted transducer geometry is that a wider substrate is needed. In the cases where neither the tilted nor the split finger geometry is acceptable, substrates with low electo-mechanical coupling coefficients, such as quartz, may be used to reduce reflections.

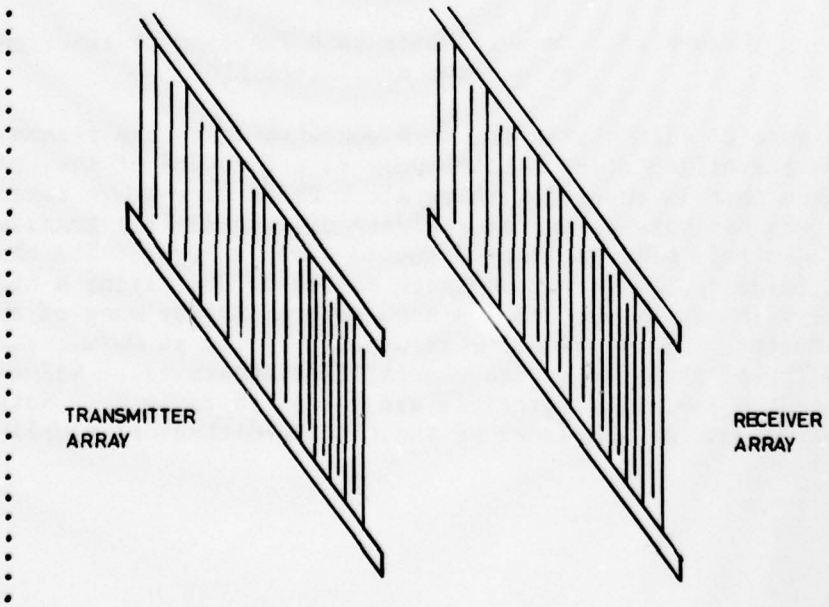

Figure 22. Schematic of a tilted transducer pair

4.6.2 Mass loading of substrate

A second, less severe source of reflections is the mass loading of the metal electrodes on the surface of the substrate. In determining the electrode thickness, the designer must trade off the resistance of the electrode with the mass loading of the electrode. Aluminium has been a very common electrode material due to its low mass density and high conductivity. Typical thicknesses for aluminium are of the order of a few thousand Angstrom units. An alternative electrode metal which has been extensively used is gold which is usually deposited in thinner layers than is aluminium. The split fingered and tilted geometries reduce the effect of reflections generated due to this cause also. Mechanical reflections in interdigital transducers have been analysed by Skeie [49].

4.7 Wave velocity changes due to surface metallisation

The presence of metal electrodes on the surface of a piezo-electric substrate causes a slowing of the surface wave velocity due to the short circuiting of piezo-electric field.

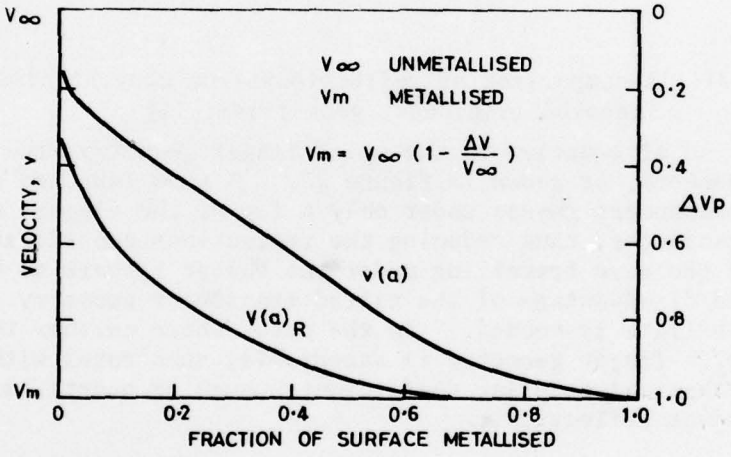

Figure 23. Wave velocity as a function of fraction of surfave metallised [56]

Figure 23 illustrates the mean phase velocity and resonance velocity of waves travelling under a transducer as a function of the fraction of surface that is covered with metal. These curves are taken from Emtage [56] who has carried out an analysis of interdigital transducers which includes this often neglected second order effect. The change in surface wave velocity, Δv, of a substrate caused by depositing a high conductive metal film on the surface has been determined for many of the common substrates. This parameter is usually listed as $\Delta v/v_{oo}$, v_{oo} being the velocity of the wave on the unmetallised substrate. Values of $\Delta v/v_{oo}$ for the common substrate materials are listed in Table 1. Note that $\Delta v/v_{oo}$ is often used as a measure of the electro-mechanical coupling coefficient.

TABLE 1. ACOUSTIC SURFACE WAVE MATERIAL DATA

MATERIAL	$LiNbO_3$	$LiNbO_3$	$LiNbO_3$	$LiNbO_3$	$LiNbO_3$	$Bi_{12}GeO_{20}$	$Bi_{12}GeO_{20}$	$Bi_{12}GeO_{20}$	$LiTaO_3$	$LiTaO_3$	$LiTaO_3$	Quartz	Quartz	GaAs	GaAs	$Ba_2NaNb_5O_{15}$
ORIENTATION	Y Cut Z Prop	16 1/2° double rotated cut	41 1/2° Rotated Cut X Prop	Z Cut X Prop	X Cut Z Prop	001 Cut 110 Prop	111 Cut 110 Prop	110 Cut 001 Prop	Z Cut Y Prop	Y Cut Z Prop	22° Rotated Cut X Prop	Y Cut X Prop	ST Cut X Prop	110 Cut X Prop	211 Cut 111 Prop	Y Cut Z Prop
SURFACE WAVE VELOCITY, V_{00} (m/sec)	3488	3503	4000	3798	3483	1681	1708	1624	3329	5230	3302	3159	3158	2822	2621	3177
ESTIMATE OF ELECTROMAGNETIC TO ACOUSTIC COUPLING, $\Delta V/V_{00}$	0.0241	0.0268	0.0277	0.0026	0.0252	0.0068	0.0082	0.0037	0.0759	0.0053	0.0027	0.0009	0.00050	0.00008	0.00012	0.0085
POWER FLOW ANGLE ϕ (deg) (ELECTROMECHANICAL)	0	0	0	0	-1.726	0	0	0	0	0	0	0	0	0	0	0
TEMPERATURE COEFFICIENT OF DELAY $\frac{1}{T}\frac{\partial T}{\partial T}$ (ppm)	94.	96.	72.	77.	93.	—	—	—	69.	35.	68.	-24.	0.	—	—	—
SW ATTN IN AIR AT 1GHz* (dB/μsec)	1.07	1.15	1.05	0.93	—	1.64	1.64	—	1.0	1.14	—	2.6	3.09	4.22	3.62	~3.7
AIR LOADING AT 1GHz* (dB/μsec)	0.19	0.21	0.3	0.24	—	0.19	0.19	—	0.23	0.20	—	0.45	0.47	0.49	0.27	—
VAC ATTN AT 1GHz* (dB/μsec)	0.88	0.94	0.75	0.69	—	1.45	1.45	—	0.77	0.94	—	2.15	2.62	3.88	3.35	—
3 dB AIR PROP LOSS TIME DELAY AT 1GHz*, A (μsec)	2.8	2.6	2.9	3.2	—	1.8	1.8	—	3.0	2.6	—	1.2	0.97	0.71	0.83	~0.8
SLOPE OF ELECTROMECHANICAL POWER FLOW CURVE, $\partial\phi/\partial\theta$	-1.083	-1.087	-0.445	+0.192	-0.610	-0.304	+0.306	+0.236	-1.241	-0.211	+0.764	+0.653	+0.378	-0.537	-2.98	+0.071
SLOPE OF ELECTROMECHANICAL POWER FLOW CURVE, $\partial\phi/\partial\mu$	-0.117	+0.151	0	0	0	0	0	0	+0.556	-0.229	0	0	0	0	0	0
3dB BEAM STEERING LOSS TIME DELAY, ^1B (μsec)	5.19	4.98	15.08	34.99	11.00	22.08	18.34	20.64	2.94	10.09	8.79	10.28	17.76	12.50	2.60	94.54
3dB DIFFRACTION LOSS TIME DELAY AT 1 GHz, ^1C (μsec)	29.1	29.3	5.1	2.4	7.6	4.1	2.1	2.3	11.3	3.6	1.6	1.7	2.1	0.1	1.50	2.65
MATERIAL FIGURE OF MERIT $F_M = ABC(\frac{\Delta V}{V_{00}})^2$	0.246	0.268	0.171	0.0018	—	0.0075	0.0047	—	0.0035	0.0010	—	1.7×10^{-5}	1.2×10^{-5}	3.5×10^{-7}	4.7×10^{-8}	—
TIME - BW PRODUCT FIGURE OF MERIT $F_{TB} = \frac{8M^2ABC}{V_{00}}(\frac{\Delta V}{V_{00}})^2$	0.788	0.386	0.171	0.0019	—	0.018	0.011	—	0.0042	0.0013	—	2.2×10^{-5}	1.5×10^{-5}	4.9×10^{-7}	7.1×10^{-8}	—

Courtesy of Air Force Cambridge Research Laboratories

The effects of velocity changes due to surface metallisation are most severe in apodised structures, where different sections of the wave front pass under different amounts of metal, thus causing some of the wave front to be retarded more than the rest. Tancrell and Williamson [53], have overcome this problem by the use of dummy fingers which do not interact with the wave but provide the whole wave front with an equal amount of metal to pass under (see figure 24). This effect is more prominent in substrates with high electro-mechanical coupling coefficients such as Lithium Niobate.

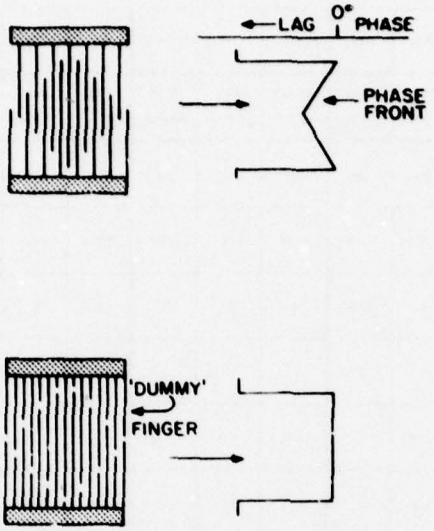

Figure 24. A comparison of wavefront and distortion with and without compensating dummy electrodes

4.8 Effects of crystal anisotropy

The materials commonly used for surface acoustic wave substrates are anisotropic crystals. This means that fundamental physical quantities, such as velocity, power flow angle, electro-mechanical coupling coefficient and other electrical and mechanical parameters, are functions of the direction of propagation. The effects of crystal anisotropy are well covered in [50] and [51], however, in the interest of completeness, they will be covered briefly here.

4.8.1 Velocity anisotropy

The obvious effect of velocity anisotropy is the change in fundamental frequency for taps placed at a given spacing. A less obvious effect is the change in electro-mechanical coupling coefficient k with direction. The electro-mechanical coupling coefficient is defined as the ratio of mutual elastic and dielectric self energies. The coupling coefficient for a given configuration is relatively difficult to determine directly; but it may be obtained from a knowledge of the change in wave velocity due to a change in the electric field boundary conditions. A simplified expression for the coupling coefficient:

$$k^2 \doteq 2 \left| \Delta v / v_\infty \right| \qquad \ldots.(9)$$

Curves of surface wave velocity and $\Delta v/v_\infty$ versus plate normal direction for Lithium Niobate are illustrated in figures 25 and 26. These curves will give the designer some idea as to the tolerance to specify for the substrate crystal orientation for a given device.

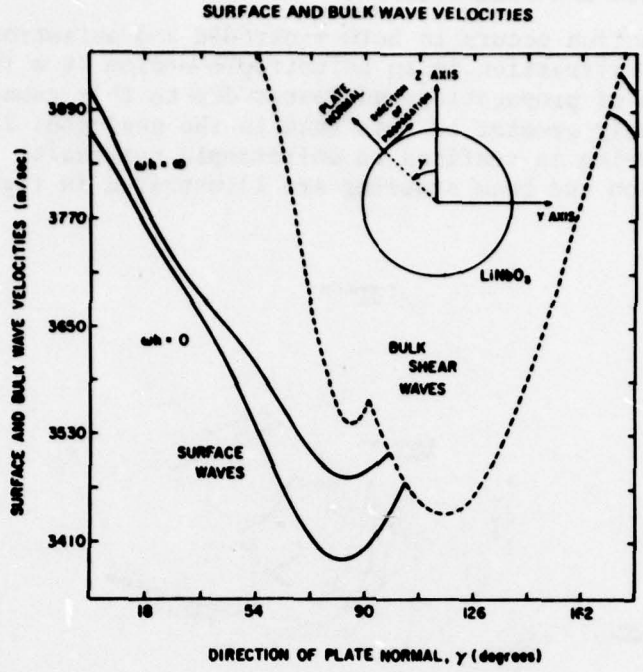

Figure 25. Surface and bulk wave velocities as a function of direction of plate normal [51]

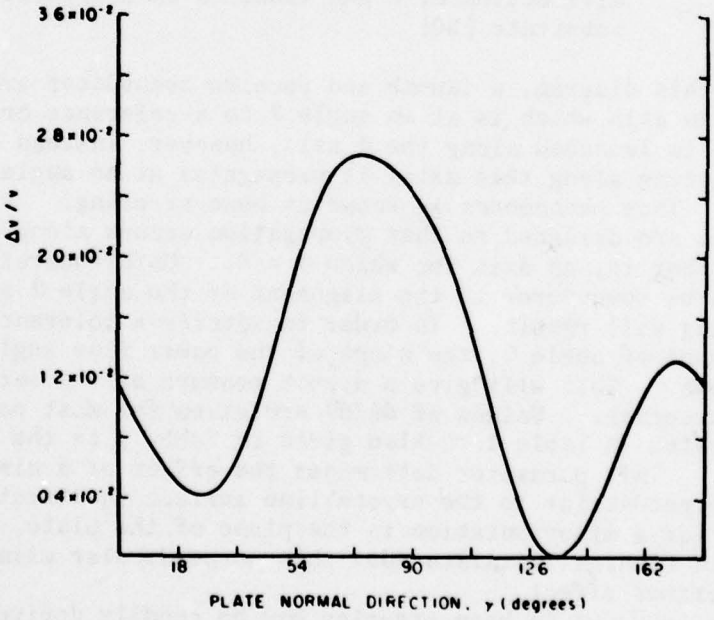

Figure 26. $\Delta v/v_{oo}$ as a function of direction of plate normal [50]

4.8.2 Diffraction and beam steering

Diffraction occurs in both isotropic and anisotropic materials. However, diffraction in an anisotropic medium is a function of the direction of propagation and losses due to this cause may be considerably greater or less than in the analogous isotropic case. Beam steering is confined to anisotropic materials. Both diffraction and beam steering are illustrated in figure 27.

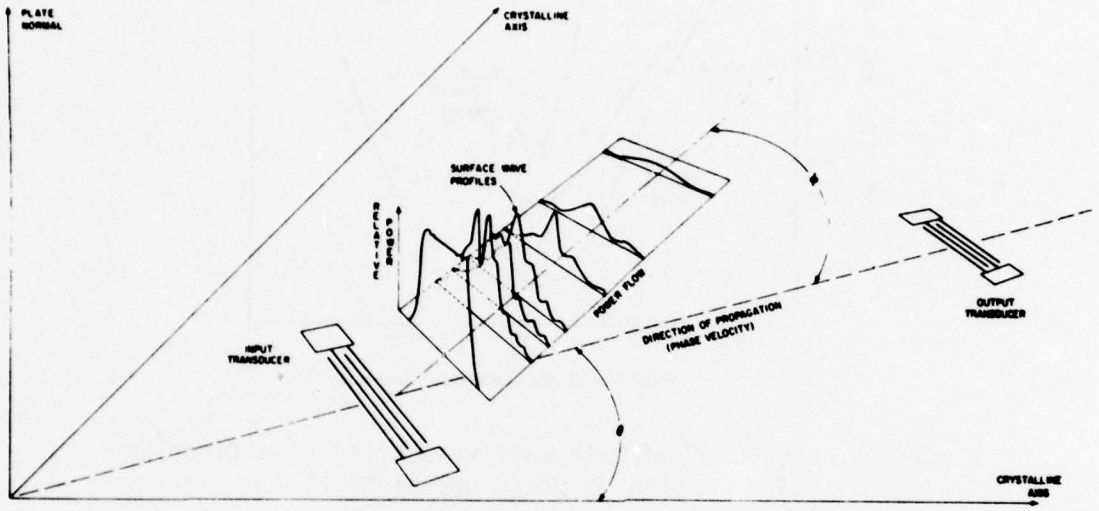

Figure 27. Schematic representation of beam steering and diffraction of a SAW launched on a crystalline substrate [50]

In this diagram, a launch and receive transducer are each placed along an axis which is at an angle θ to a reference crystalline axis. A wave is launched along the θ axis, however, instead of the power propagating along this axis, it propagates at an angle of ϕ to this axis. This phenomenon is known as beam steering. Practical devices are designed so that propagation occurs along a pure mode axis, that is, an axis for which $\phi = 0$. Unfortunately, there will always be some error in the alignment of the angle θ and some beam steering will result. In order to specify a tolerance on the alignment of angle θ, the slope of the power flow angle $d\phi/d\theta$ must be known. This will give a direct measure of the seriousness of beam steering. Values of $d\phi/d\theta$ are given for most popular substrates in Table 1. Also given in Table 1 is the parameter $d\phi/d\mu$. This parameter determines the effect of a misorientation of the perpendicular to the crystalline surface in direct analogy with $d\phi/d\theta$ for a misorientation in the plane of the plate. Note that only in Lithium Tantalate does this perpendicular misalignment have any serious effect.

The loss due to beam steering may be readily derived by simple geometric methods.

Beam steering loss (db) = $-20 \log_{10} (1 - \Delta\theta |d\phi/d\theta| \hat{\ell}/\hat{L})$ ....(10)

where = alignment error of crystalline axis (radians)

$\hat{\ell}$ = distance between launch and receive transducers (wavelengths)

$\hat{L}$ = transducer width (wavelengths)

Diffraction, illustrated in figure 27 by the changing beam profile and eventual beam spreading, is also a function of crystal orientation and must be considered simultaneously with beam steering. In fact, the designer must trade off the losses caused by each of these in order to optimise a particular design. A thorough treatment of diffraction is given by Szabo and Slobodnik [51].

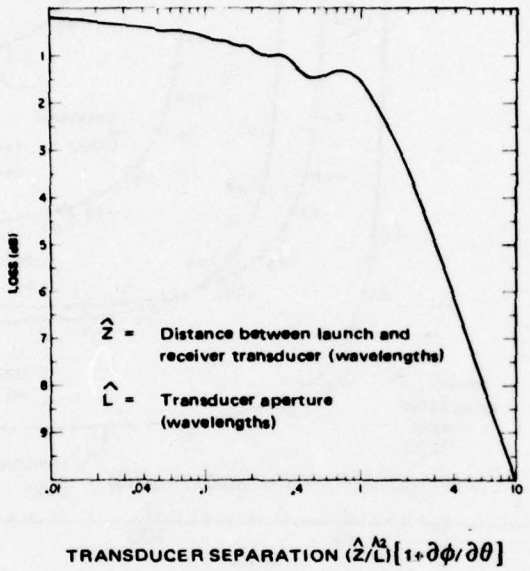

Figure 28. Diffraction loss versus scaled transducer separation [51]

Diffraction loss is illustrated in figure 28 which is a universal diffraction loss curve for all parabolic materials (materials for which velocities near the pure mode axes can be approximated by parabolas). The use of these curves for the known non-parabolic surface wave substrates leads to only slight errors. The near field diffraction loss never exceeds 1.6db (the near field being defined as $\hat{z} < \hat{L}^2 / |1 + \partial\phi/\partial\theta|$). The far field diffraction loss may be expressed as:

$$\text{Far Field Diffraction Loss (db)} = -10 \log_{10} x - 1.6/x^2 \quad \ldots(11)$$

where $x = \hat{z} / \hat{L}^2 \; | \; 1 + \partial\phi/\partial\theta \; |$

The above expression is valid for: $\hat{z} \geq \hat{L}^2 / | \; 1 + \partial\phi/\partial\theta \; |$

Figure 29 illustrates the trade off obtained by simultaneously plotting beam steering and diffraction losses. Several values of transducer width and frequency are included. The parameter $d\phi/d\theta$ may be obtained from Table 1 and superimposed upon figure 29 to obtain a comparison of trade-offs for the common substrates. It may be seen that by increasing transducer lengths and decreasing the operating frequency, beam steering may be made negligible for the lengths of substrate currently available.

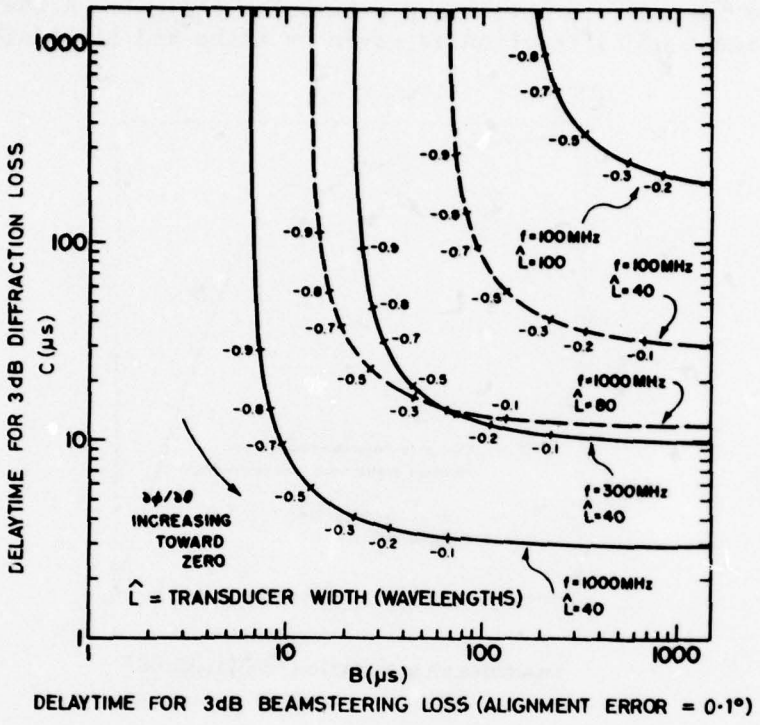

Figure 29. Trade-off between diffraction loss and beam steering loss [50]

4.9 Temperature effects

When consideration is being given to the design of a surface wave correlator for long phase coded sequences, etc., the temperature coefficient of surface wave delay can be the limiting parameter in determining the peak to sidelobe ratio. The temperature coefficient of delay is a function of both temperature coefficient of linear expansion and temperature coefficient of surface wave velocity. Unfortunately, most common substrates have a positive temperature coefficient of linear expansion and a negative temperature coefficient of wave velocity, resulting in a nett positive temperature coefficient of delay. A notable exception to this is quartz which has a negative temperature coefficient of delay for the Y cut, X propagating substrate and a zero first order temperature coefficient of delay for the ST cut, X propagation substrate. See figure 30. Temperature coefficients of delay for the common surface acoustic wave substrates are given in Table 1.

Investigations are being carried out to develop a temperature stable, high coupling coefficient surface acoustic wave device. A number of approaches have been used, one involves the depositing of a resistive material on the substrate, through which a current is passed to keep the substrate at a constant temperature. Another approach has been to use a thin layer of one material on a second substrate material, the two materials having counteracting thermal properties.

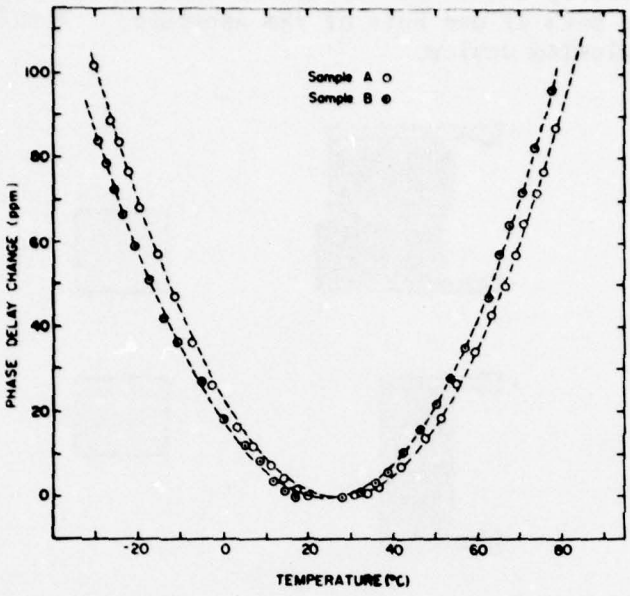

Figure 30. Phase delay as a function of temperature for ST cut quartz [48]

4.10 Bulk wave generation

In the generation of surface acoustic Rayleigh waves, both shear and longitudinal strains are set up by the launch transducer. Instead of all of this strain energy propagating as surface waves, some of it may propagate away from the excitation region as bulk waves. Direct bulk wave generation may also occur if an earth plane is located on the opposite side of the substrate to the launch transducer. The most serious of the bulk wave responses are the ones occurring within the surface wave passband. These cause spurious responses which are typically 20db to 50db below the desired responses and place serious limits on high performance devices.

Bulk wave excitation in anisotropic crystals, like surface wave excitation, is a function of crystal axis orientation. Fortunately, the axis of maximum surface wave coupling and the axis of maximum bulk wave coupling are not necessarily collinear (see figure 25). Selection of the correct crystalline axis is a major factor in reducing bulk wave responses [47].

Interdigital transducers may excite both shear and longitudinal bulk waves. At the higher frequencies, the shear bulk waves will be directed from the top surface of the substrate to the bottom surface where they will be reflected. Roughening the bottom surface will help to scatter this wave. A more effective method is to machine the reverse side of the device so that it forms an angle with the top surface. This causes bulk waves which are reflected from the bottom surface to be skewed on arrival at the output transducer [54]. Another method of reducing bulk wave spurious responses is by the use of the split electrode transducer geometry - this prevents reflected energy from being scattered into bulk waves at the frequencies of interest.

In the past, bulk wave generation has been a major problem in the implementation of highly dispersive filters. La Rose and Vasile, [44], have demonstrated a method of bulk wave cancellation using a launch transducer which is split in two (figure 31); the two halves being phased

so that bulk waves generated by each half cancel, whilst the two surface waves generated by these transducers are phased up by placing a slowing device in the path of one half of the aperture. A thin metal coating is used as the slowing device.

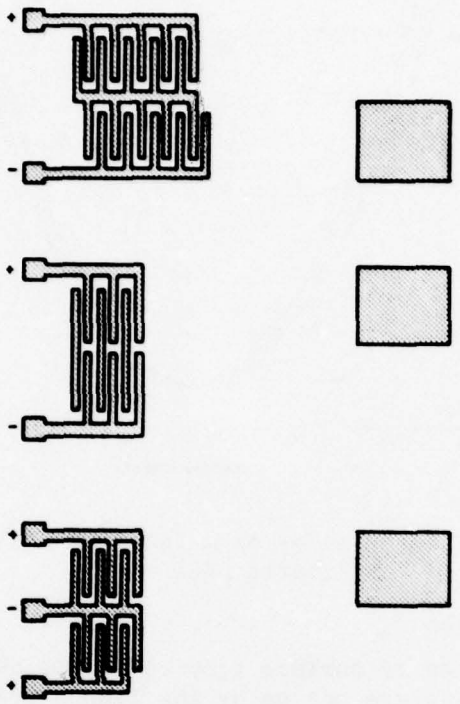

Figure 31. Transducer geometry for bulk wave cancellation [44]

Bulk wave responses may be considerably reduced by placing launch and receive transducers on adjacent tracks with a multistrip coupler [63] coupling between these tracks. The multistrip coupler will cause the surface wave to change tracks but will leave the bulk wave on its original track, thus missing the receive transducer. Unfortunately multistrip coupler lengths become impracticable on low coupling coefficient substrates such as quartz.

4.11 Direct transducer to transducer feedthrough

In practical surface acoustic wave devices, insertion losses of 40db or more may be typical, particularly in the case of phase coded transducers which use ST cut quartz for its zero first order temperature coefficient of delay. Quartz has a low electro-mechanical coupling coefficient, and for devices which have more than five percent fractional bandwidth must be damped to realise the desired bandwidth, which implies high insertion loss. If no precautions are taken in these high insertion loss devices, then direct feedthrough between the input and output transducers may produce a larger signal than the desired acoustically coupled signal. Direct feedthrough may be kept to a level of about -70db with careful layout and shielding, or with a great deal of attention to earthing and special shielding 100db of isolation may be achieved. Isolation has been found to improve as transducer separation is increased as would be expected from normal capacitive coupling theory. By placing an earthed cap over a device, isolation is found to improve with closeness of the cap to the device, with good isolation (60 - 70db at 150 MHz) occurring with a spacing of about 0.25 to 0.5 mm.

5. TRANSDUCER ANALYSIS

The electric field at any point in an interdigital transducer is the sum of the field due to the exciting voltage applied to that transducer and the field associated with the wave travelling under that transducer. The field associated with the wave travelling under the transducer is complex being modified by reflections from each finger pair it passes under.

Smith et. al. [68], have carried out a simplified analysis of interdigital transducers which assumes the surface wave substrate is non-piezo-electric in that there are no reflections between finger pairs and the electric forcing field is not modified by the field of the existing surface waves. The distortion in transducer response caused by neglecting these 'piezo-electric feedback' effects is shown in figure 32.

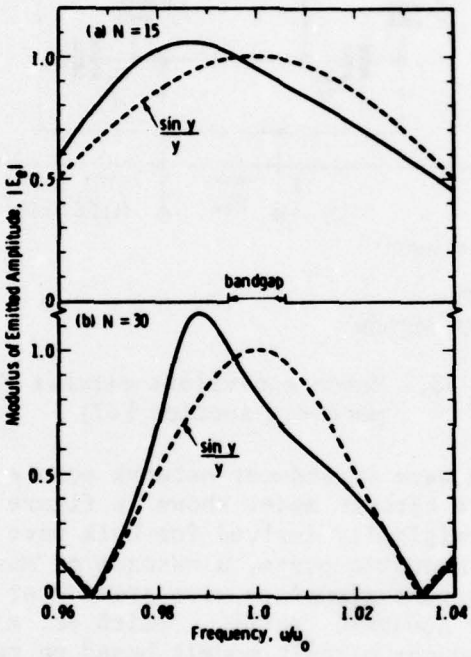

Figure 32. Distortion of ideal sin y/y response caused by reflection at finger edges [56]

Ingebrigtsen, [62] and Emtage, [56], have both carried out analyses of interdigital transducers which include the 'piezo-electric feedback' effects. Both analyses agree well with experimental results. (Note that this distortion does not occur with split fingers as the reflection from finger edges tend to cancel.) Although it is desirable to be able to accurately predict the effects of 'piezo-electric feedback' or for that matter any second order effect, it is even more desirable to eliminate these second order effects (by the methods discussed in the previous sections). If these second order effects can be reduced to a level where they do not have any appreciable effect on the transducer response, then the simplified analysis of Smith et. al. may be used with good results.

5.1 Equivalent circuit models

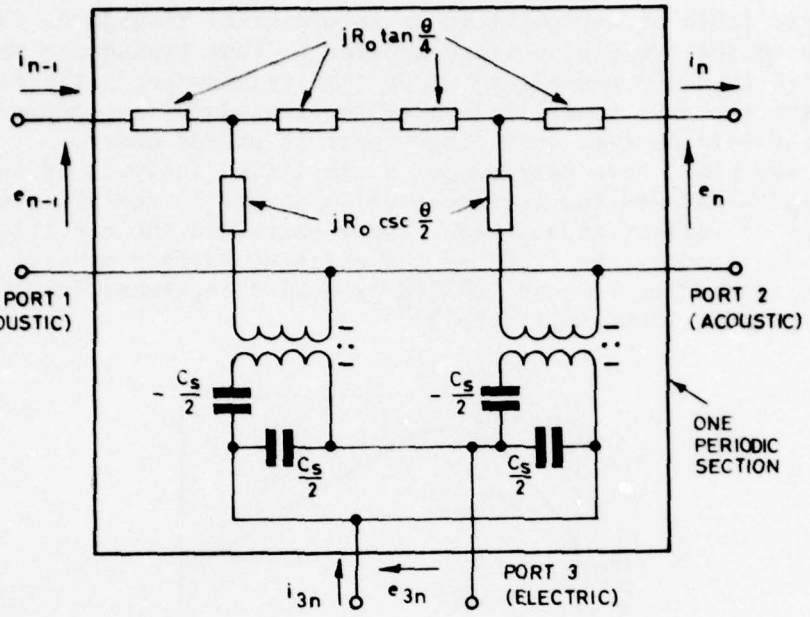

$\theta = 2\pi\, w/w_o$ = PERIOD SECTION TRANSIT ANGLE

R_o = ELECTRICAL EQUIVALENT OF Z_o

C_s = ELECTRODE CAPACITANCE PER SECTION

Figure 33. Mason equivalent circuit for one periodic section [67]

Surface acoustic wave transducer network models are based on the Mason three port bulk wave circuit model shown in figure 33. Although this circuit model was originally derived for bulk wave transducers having one electrical and two acoustic ports, a cascade of Mason equivalent circuits may be used to represent a surface wave transducer which has one electrical and many acoustic ports. Smith et. al. [68], have proposed two different transducer circuit models based on two different electric field approximations; the 'crossed field' model which assumes the dominant electric field is normal to the surface of the substrate and the 'in line field' model which assumes the dominant electric field is along the surface of the substrate - see figure 34.

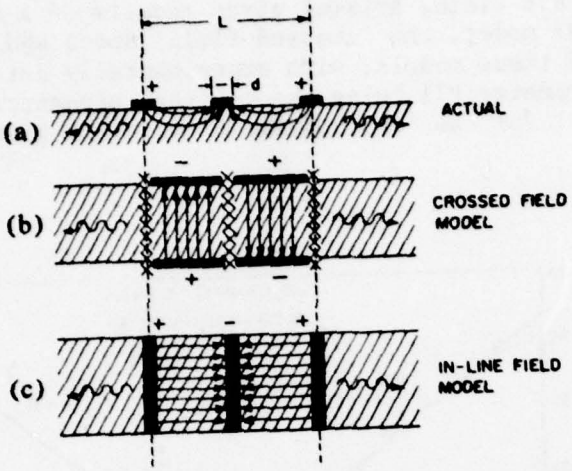

Figure 34. 'Crossed field' and 'in line field' approximations to actual transducer electric field

There is some disagreement amongst various researchers as to which is the correct circuit model to use under which circumstances. Holland and Claiborne [2], conclude that the 'crossed field' model should be used for Lithium Niobate (high electro-mechanical coupling coefficient) with a large number of fingers and the 'in line' model should be used for Quartz (low electro-mechanical coupling coefficient) with a small number of fingers. Smith et. al. [68], have published empirical results, shown in figure 35 which support the use of the 'crossed field' model for Lithium Niobate.

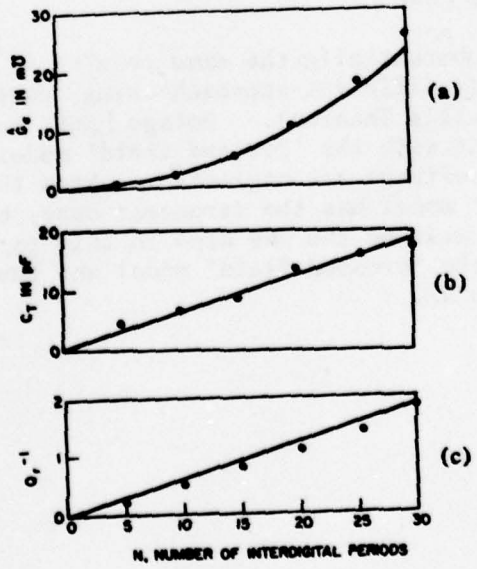

Figure 35. A comparison of empirical results with theoretical values from the 'crossed field' model [67]

Milsom and Redwood [65], have proposed a model intermediate between the 'crossed field' and the 'in line field' models and claim that this model best suits the particular polarised ceramic PZT4. Bristol [55], is quite adamant that the 'crossed field' model is the only model to be used and claims that the use of any other model will result in significant errors. In support of his claim, Bristol gives results of a comparison of the 'in line field' model, the 'crossed field' model and a model consisting of 50% of each of these models, with experimentally determined results, the scattering parameter P11 being the critical parameter - see figure 36. Further support for the 'crossed field' model is given by Hartmann et. al.

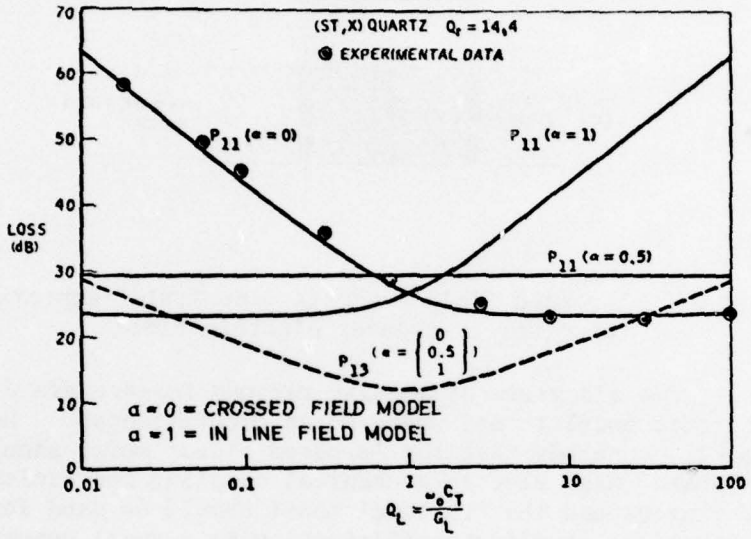

Figure 36. Experimentally determined scattering parameters compared with results from 'in line' and 'crossed field' circuit models [55]

[20] who derives substantially the same results as the 'crossed field' model by an entirely different approach using conservation of energy principles (Parsavall's Theorem). Emtage [56], has derived results which are consistent with the 'crossed field' model, providing that 'piezo-electric feedback' effects are neglected. From the above, it appears that the 'crossed field' model has the strongest case, both empirically and theoretically, and will be the one used in this paper. Equivalent circuits for both the 'crossed field' model and the 'in line field' model are given in figure 37.

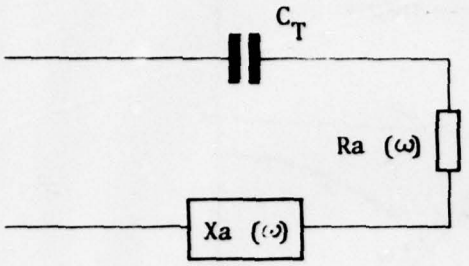

'In Line Field' Model

$$Ra\ (\omega) = Ra\ (\omega\ o)\left(\frac{\sin x}{x}\right)^2$$

$$Xa\ (\omega) = Ra\ (\omega\ o)\left(\frac{\sin 2x - 2x}{2x^2}\right)$$

$$Ra\ (\omega\ o) = \left(\frac{4}{\pi}\right)k^2\ (\omega\ oCs)^{-1}$$

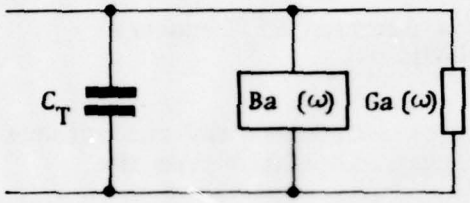

'Crossed Field' Model

$$Ga\ (\omega) = Ga\ (\omega\ o)\left(\frac{\sin x}{x}\right)^2$$

$$Ba\ (\omega) = Ga\ (\omega\ o)\left(\frac{\sin 2x - 2x}{2x^2}\right)$$

$$Ga\ (\omega\ o) = \left(\frac{4}{\pi}\right)k^2\ (\omega\ oCs)N^2$$

where $C_T = NCs$

$$x = N\pi\left(\frac{\omega - \omega\ o}{\omega\ o}\right)$$

Figure 37. Equivalent circuits for the 'in line field' and 'crossed field' models

Their immittances may be expressed as:

For the 'in line field' series equivalent circuit:

$$Ra\ (\omega) = Ra\ (\omega\ o)\ (\sin x/x)^2 \quad \ldots.(12)$$

$$Xa\ (\omega) = Ra\ (\omega\ o)\ (\sin 2x - 2x)/2x^2 \quad \ldots.(13)$$

$$Ra\ (\omega\ o) = (4/\pi).k^2/\omega\ oCs \quad \ldots.(14)$$

For the 'crossed field' shunt equivalent circuit:

$$Ga\ (\omega) = Ga\ (\omega\ o)\ (\sin x/x)^2 \quad \ldots.(15)$$

$$Ba\ (\omega) = Ga\ (\omega\ o)\ (\sin 2x - 2x)/2x^2 \quad \ldots.(16)$$

$$Ga\ (\omega\ o) = (4/\pi).k^2\ \omega\ oCsN^2 \quad \ldots.(17)$$

where $x = N\pi\ (\omega - \omega\ o)/\omega\ o$

and Cs = capacitance per periodic section

$C_T = N.Cs$ total transducer capacitance

N = number of periodic sections

k = electro-mechanical coupling coefficient

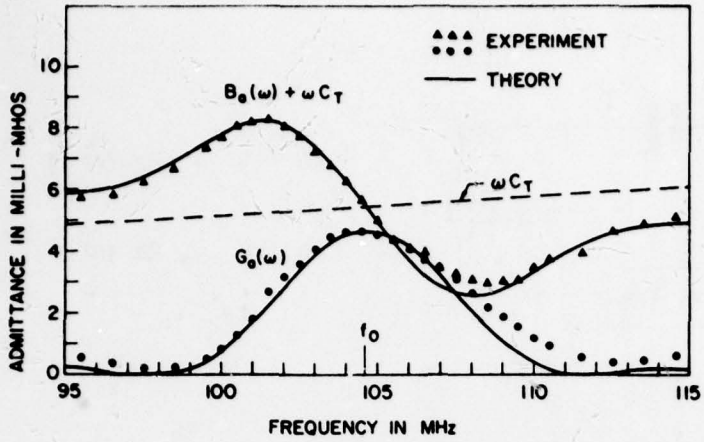

Figure 38. Radiation admittance as a function of frequency (crossed field theory) [67]

Figure 38 illustrates the measured radiation admittance and susceptance as a function of frequency compared with that calculated from the 'crossed field' model (from [68]).

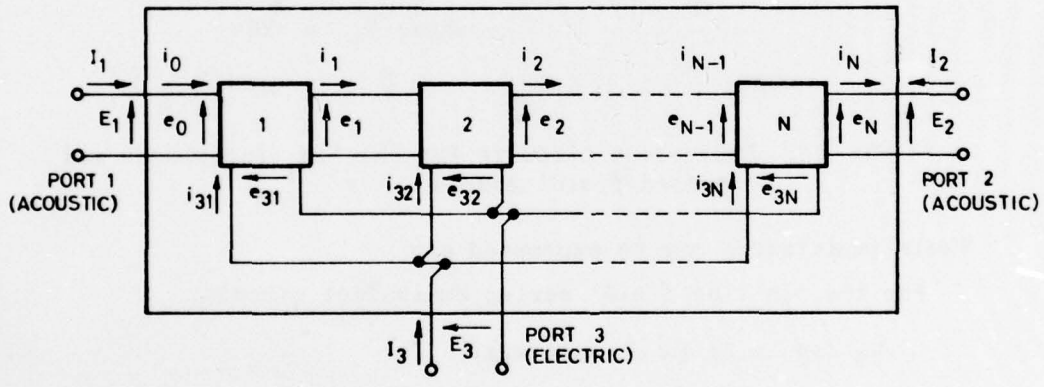

Figure 39. Transducer composed of N periodic sections, acoustically in cascade and electrically in parallel

A transducer may be treated as a network of Mason equivalent circuits, the most simple of which is the uniform unapodized transducer which is depicted in figure 39 as a cascade of Mason circuits. The analysis of apodized transducers has been treated by Tancrell and Holland [25], in this case the transducer comb is cut into lateral imaginary strips as in figure 40, these strips are used to determine which of the electrodes interact acoustically and the equivalent circuit of figure 41 is then derived.

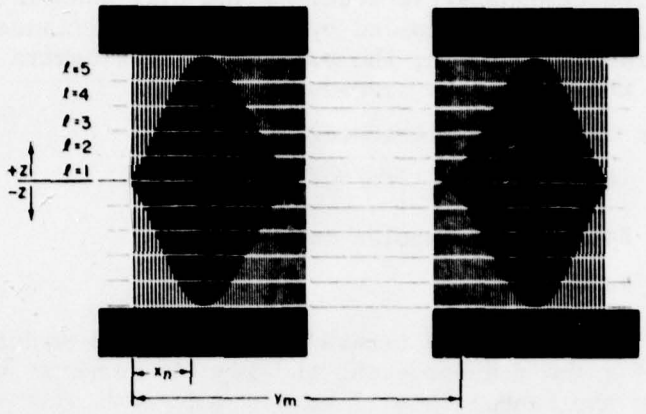

Figure 40. Apodized transducer cut into lateral imaginary strips to aid analysis [12]

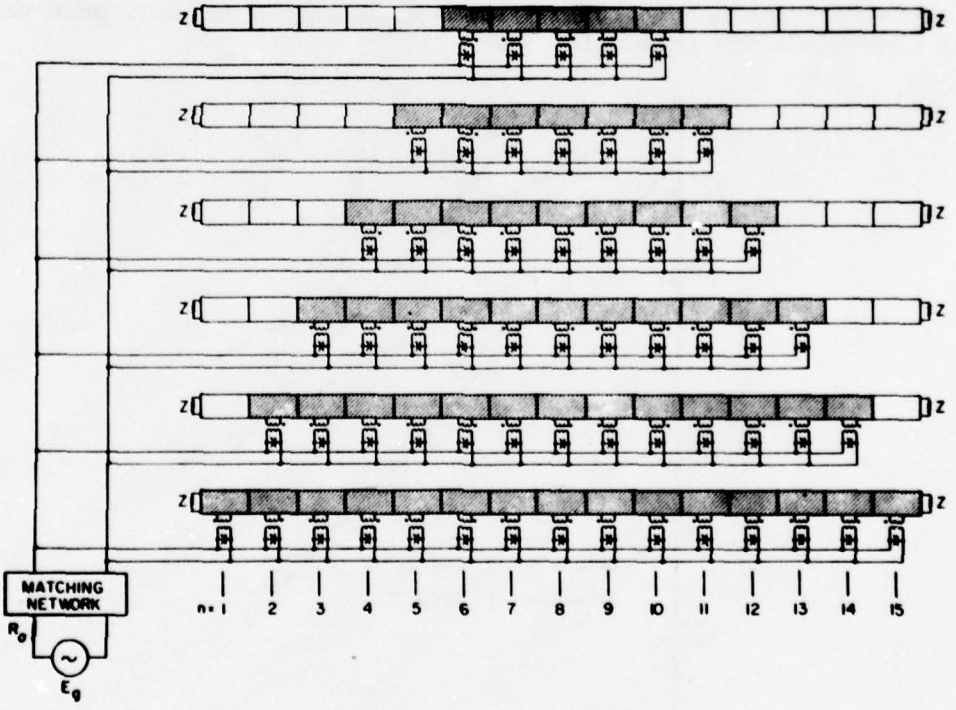

Figure 41. Equivalent circuit for an apodized transducer [12]

The analysis of dispersive surface wave devices, such as phase coded correlators and linear FM pulse compression filters, has been carried out by Hartmann et. al. [20]. It has been shown that the input admittance of a dispersive transducer is equal to the time-bandwidth product of the dispersive transducer multiplied by the input admittance of a non dispersive transducer having the same bandwidth, centre frequency and beamwidth as the dispersive transducer.

Thus for a dispersive transducer:

$$G(\omega o) = (4/\pi)k^2 \omega o C_s (fo/\Delta f)^2 \tau \Delta f \quad \ldots.(18)$$

where τ = duration of impulse response

Δf = Bandwidth

For the case of phase coded transducers which have widely spaced taps consisting of a few fingers each, the impulse response will be a train of RF bursts and the bandwidth will be the bandwidth of a single tap. The fractional bandwidth ($\Delta f/fo$) of a tap consisting of N finger pairs should be taken as 1/N. If each tap in the transducer is a single finger pair then it will have a time-bandwidth product of unity and the time-bandwidth product of the entire transducer will be equal to the number of taps. Hartmann has also derived a set of universal admittance curves for transducers on both Quartz and Lithium Niobate. These curves shown in figure 42 are for non-dispersive transducers with an acoustic beamwidth of 100 wavelengths and should be scaled to actual device bandwidth. Dispersive transducers may be treated by multiplying admittance values by the time-bandwidth product.

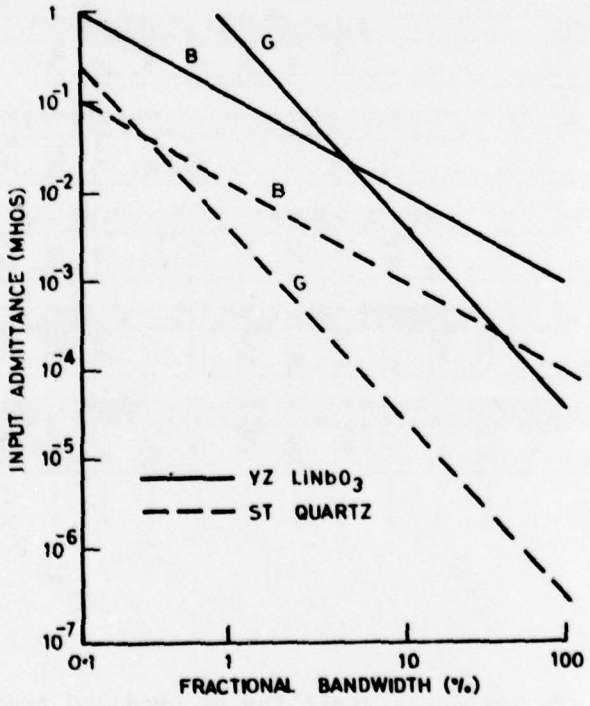

Figure 42. Input admittance for approximately rectanguar band-pass characteristics for an assumed beam width of 100 λ [20]

5.2 Electrical matching network

For minimum device insertion loss, the source immittance should be the complex conjugate of the input transducer immittance and the load immittance should be the complex conjugate of the output transducer immittance. To achieve maximum bandwidth, for a fixed number of fingers N the Q of the radiation immittance should be minimised. The radiation Q of the 'crossed field' model and the 'in line field' model may be expressed as:

$$Q_r = 1/\omega_o C_T \, Ra(\omega_o) \quad \text{'in line field' model}$$

$$Q_r = \omega_o C_T/Ga(\omega_o) \quad \text{'crossed field' model}$$

By substitution, both of the above expressions simplify to:

$$Q_r = \pi/(4Nk^2) \qquad \ldots.(19)$$

This indicates that the material with the highest coupling coefficient will have the maximum fractional bandwidth under minimum insertion loss conditions.

To a first order approximation, the overall bandshape of a surface wave device may be considered as the product of the electrical bandshape and the transducer acoustic bandshape, the transducer acoustic bandshape being determined by taking the inverse Fourier transform of the electrode pattern. This implies that the overall bandshape is determined by the smaller bandshape of the two and also that, for maximum bandwidth under minimum insertion loss conditions, the transducer electrical Q should equal the transducer acoustic radiation Q.

Consider the case of an unapodized transducer consisting of N periodic sections, of $\lambda = V/f_o$ each, as in figure 43.

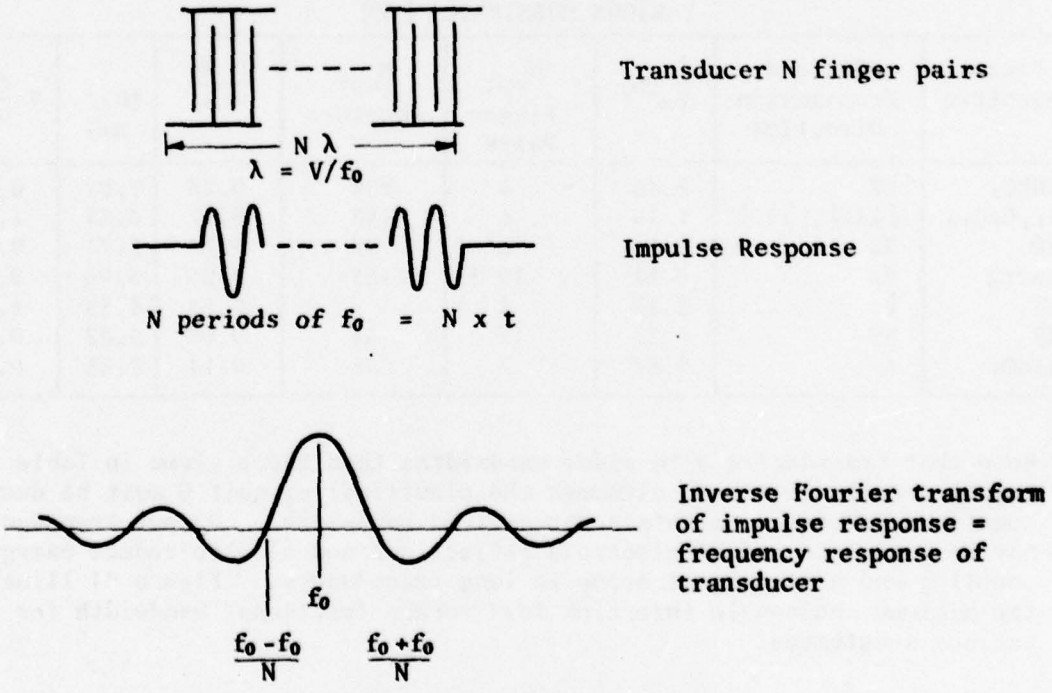

Note: fractional bandwidth between units = 2/N
$Q \approx N$

Figure 43. Transducer geometry, impulse response and frequency response

As there is a one to one correspondence between the transducer finger location and its impulse response, the latter will be a pulse train consisting of N cycles of frequency f_0. The inverse Fourier transform of this impulse response will be the transducer frequency response which, for this case, is the familiar sin x/x response centred about f_0. The zero crossings of the sin x/x pattern occur at multiples of 1/T where T is the duration of the pulse train.

Now $T = N.t = N/f_0 = N\lambda/V$

where t is the period corresponding to a frequency f_0

V is surface wave velocity

Thus the first nulls in the transducer frequency response occur at $f_0 \pm f_0/N$ or the fractional bandwidth between the nulls = 2/N. Note also that the 3db response points occur at approximately $f_0 \pm f_0/2N$ or the 'Q' of the transducer acoustic response is approximately equal to N.

Substituting N for Q_T in expression (19), thus equating the radiation Q with the transducer acoustic Q (the condition for maximum bandwidth under minimum insertion loss conditions), gives:

$$N^2 = \pi/4k^2 \qquad \ldots.(20)$$

Smith [69] has shown this condition also to be the condition for minimum phase dispersion and has determined the optimum transducer design, based on (20), for various substrates. These appear in Table 2.

TABLE 2. OPTIMUM TRANSDUCER DESIGN FOR VARIOUS SUBSTRATES [69]

Piezo-electric	Cut and Propagation Direction	$\frac{\Delta v}{V_\infty}$(%)	N_{opt} Finger Pairs	M_{opt} Aperture	$\frac{\Delta \omega}{\omega o}$	T (μs/cm)	$T.\frac{\Delta \omega}{\omega o}$
$LiNbO_3$	YZ	2.46	4	108	0.24	2.88	0.69
$Bi_{12}GeO_{20}$	[110],[$\bar{1}$10]	1.15	6	183	0.17	6.33	1.08
ZnO	XZ	0.56	8	99	0.12	3.74	0.45
Quartz	YX	0.11	19	53	0.053	3.06	0.16
PZT	†	2.15	4	-	0.23	4.55	1.04
CdS	XY	0.31	12	54	0.09	5.82	0.52
$LiTaO_3$	ZY	0.82	7	31	0.14	2.86	0.40

Note that transducers with wider bandwidths than those given in Table 2 may be readily obtained, although the electrical circuit Q must be damped, sometimes severely, to obtain the desired bandwidth. Output transducers may be loaded to reduce electrode reflections and also to reduce energy coupling and hence signal droop in long transducers. Figure 44 illustrates the minimum achievable insertion loss versus fractional bandwidth for various substrates.

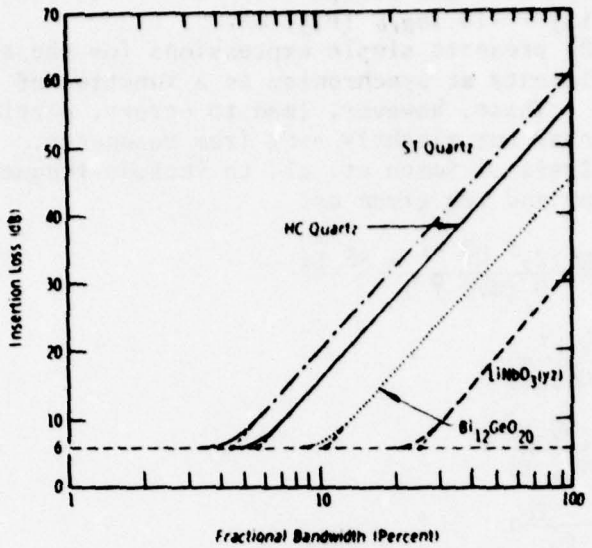

Figure 44. Minimum achievable SAW delay line insertion loss with bidirectional transducer [20]

An alternative to the matching network described above is the transmission line approach as described by Heighway et. al. [61]. In this case, the transducer is considered as a distributed network, its characteristic impedance is determined and impedance matching transformers are used to match the load and source respectively, the other end of the transducer is terminated in its characteristic impedance. The transmission line approach results in lower insertion loss than the lossless matching network for dispersive structures with high compression ratios. It also considerably simplifies the matching problem.

5.3 Transducer scattering parameters

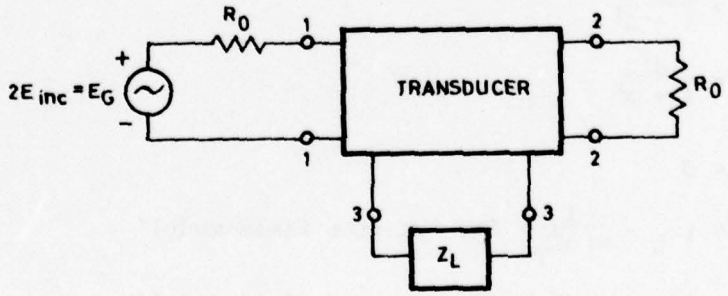

Figure 45. Scattering parameter model [67]

In order to determine the fraction of power absorbed, reflected and transmitted by a transducer from an incident surface wave, the transducer scattering parameters must be known. Using the model of figure 45, a set of power scattering coefficients will be defined for a simple unapodized transducer:

P11 = fraction of incident power reflected at port 1
P21 = fraction of incident power transmitted to acoustic port 2
P31 = fraction of incident power coupled to electrical port 3

From transducer symmetry and reciporcity P11 = P22, P13 = P23, Pij = Pij.
Scattering loss Lij = -10 $\log_{10}$ (Pij) dB.
Smith et. al. [68] presents simple expressions for the above scattering electrical coefficients at synchronism as a function of load on the electrical port. These, however, lead to errors, particularly in L11 for frequencies near but slightly away from resonance. Gerard has extended the analysis of Smith et. al. to include frequencies close to the resonant frequency and are given as:

$$P11 = \frac{1 + (N\delta/2)^2 \, |\hat{Y}|^2 - N\delta \, \hat{Y}i}{D\,(N\delta, \hat{Y})} \qquad \ldots.(21)$$

$$P21 = \frac{|\hat{Y}|^2}{D\,(N\delta, \hat{Y})} \qquad \ldots.(22)$$

$$P31 = \frac{2\,\hat{Y}}{D\,(N\delta, \hat{Y})} \qquad \ldots.(23)$$

where $\delta = 2\pi \left(\frac{f - fo}{fo}\right)$

$\hat{Y}r$ = real part of $\hat{Y}$

$\hat{Y}i$ = imaginary part of $\hat{Y}$

$\hat{Y}$ = normalised electric port load

$$= \frac{Y_L + J\,\omega\, C_T}{\hat{G}a} \qquad \ldots.(24)$$

$$Ga = (4/\pi).k^2\, \omega o\, Cs\, N^2$$

$$D\,(N\delta, \hat{Y}) = 1 + 2\,(\hat{Y}r - \hat{Y}i\, N\delta/2) + |\hat{Y}|^2\,(1 + (N\delta/2)^2)$$

For the case, f = fo (δ = 0), the above simplifies to the expressions given by Smith et. al., i.e.
For a purely reactive load at acoustic synchronism:

$$P11 = \frac{1}{1 + a^2} \qquad \ldots.(25)$$

$$P21 = \frac{a^2}{1 + a^2} \qquad \ldots.(26)$$

$$P31 = 0 \qquad \ldots.(27)$$

where $a = \left(X_L - \frac{1}{\omega\, oC_T}\right) / Ra$ 'in line field model'

$a = (B_L + \omega\, oC_t) / Ga$ 'crossed field model'

X_L = load reactance

B_L = load suspectance

For a load tuned to resonate the transducer capacitance at acoustic *synchronism:*

$$P11 = \frac{1}{(1 + b)^2} \qquad \ldots.(28)$$

$$P21 = \frac{b^2}{(1 + b)^2} \qquad \ldots.(29)$$

$$P31 = \frac{2b}{(1 + b)^2} \quad \ldots\ldots(30$$

where $b = R_L/\hat{R}a$ 'in line field model'

$b = G_L/\hat{G}a$ 'crossed field model'

R_L = load resistance

G_L = load conductance

Note that the simplified expressions of Smith et. al. are in good agreement with the more complex expressions of Gerard except for L11 and even this is in good agreement over the range b = 0.5 to 2.0 and a = -2 to +2.

Figure 46 illustrates reflection loss and transmission loss versus normalised electrical susceptance compared with Gerard's model and the model of Smith et. al.

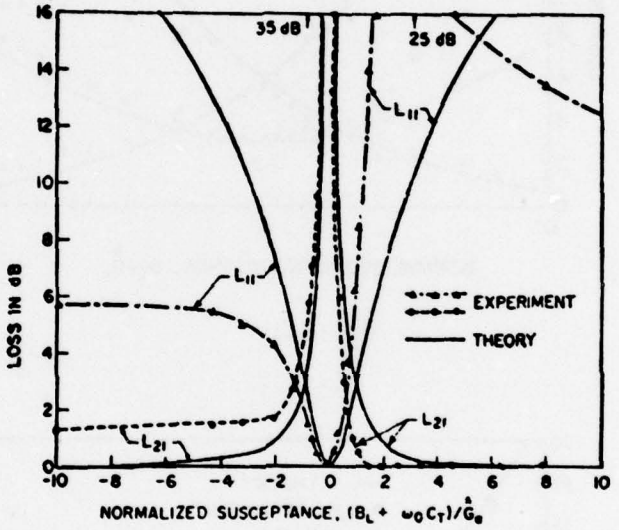

(a)

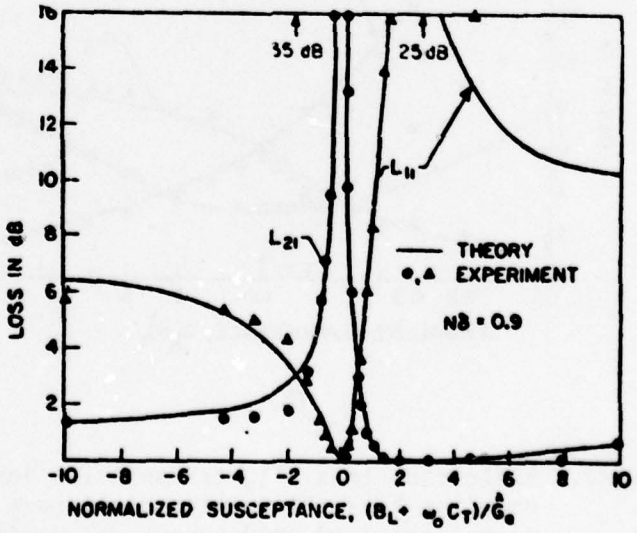

(b)

Figure 46. Reflection loss L11 and transmission loss L21 versus normalized electrical susceptance (a) Smith et. al.[68] (b) Gerard [59]

Figure 47 illustrates reflection loss, transmission loss and coupling loss versus normalised conductance for both Gerard's model and the model of Smith et. al.

Note also that the above expressions do not include reflections due to the short circuiting of the electric field by the metal electrodes. These are given in paragraph 4.6.1.

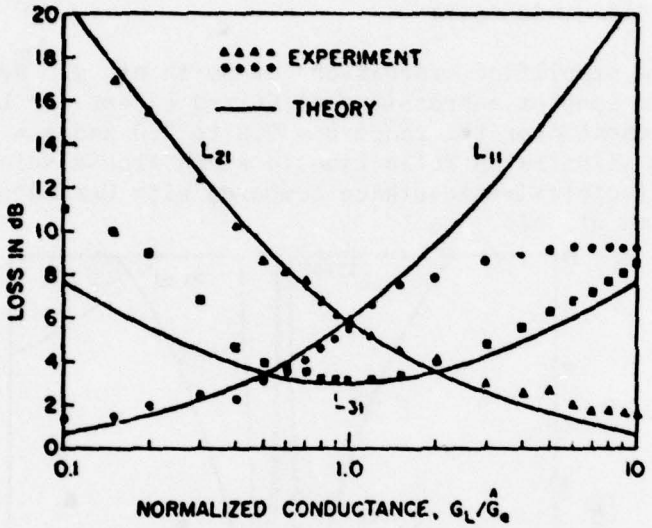

(a)

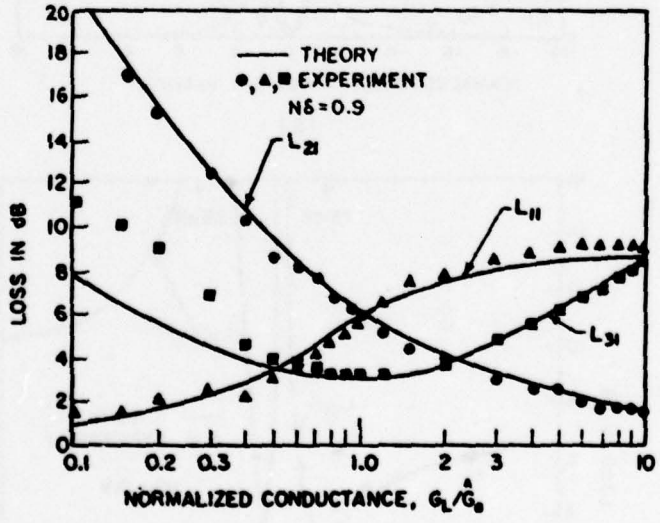

(b)

Figure 47. Reflection loss L11, transmission loss L21, and coupling loss L31 to electrical port versus normalized load conductance (a) Smith et. al. [68] (b) Gerard [59]

5.4 Transducer electrode capacitance

Farnell et. al. [58], have derived expressions for the capacitance of interdigital comb structures for a variety of configurations including layered structures, single interface structures and plated structures. Only the single interface structure, the most common structure, will be considered here. This is defined as a 'transducer deposited on the free surface of an infinitely deep substrate with alternate fingers driven in opposite phase'.

If it can be assumed that the transducer finger structure extends infinitely in both directions along the substrate surface and that the finger width is much greater than its thickness, then the capacitance of a single electrode pair may be expressed as:

$$C = (6.5\ R^2 + 1.08R + 2.37)\ (\epsilon r + 1)\ pF/m \qquad ....(31)$$

where R is the ratio of electrode width to distance between electrode centres.

ϵr is the relative dielectric constant.

For the common case where finger and gap width are equal, i.e. R = 0.5, the above expression simplifies to:

$$C = 4.53\ (\epsilon r + 1)\ pF/m \qquad ....(32)$$

For the case of phase coded sequence generators or correlators which have large gaps in between sets of taps, the capacitance may be taken as equivalent to an array with the same number of fingers as if the large gaps were not there [2].

6. TRANSDUCER DESIGN

As surface acoustic wave devices are essentially tapped delay lines, all device specifications must ultimately be transformed into the time domain. Simple delay lines and phase coded correlators are already time domain problems and are readily handled in the time domain. Filters having a certain desired band shape in the frequency domain, however, must have their response transformed into the time domain.

The impulse response of a device is the convolution of its two transducers impulse responses; or alternatively the frequency response of a device is the product of the frequency responses of its two transducers. Now as the impulse response h(t) of a device and its frequency response $H(\omega)$ are a Fourier transform pair, then its frequency response may be determined from a knowledge of its transducers electrode patterns and hence impulse responses.

$$H(\omega) = \int_{-\infty}^{+\infty} h(t)\ \exp\ (-j\omega\ t)\ dt$$

To obtain a desired frequency response, the inverse Fourier transform of the response is taken, giving the impulse response which may then be used to determine electrode position and overlap.

$$h(t) = \frac{1}{2\pi} \int_{-\infty}^{+\infty} H(\omega)\ \exp\ (j\omega\ t)\ d\omega$$

A limitation in practice is that the impulse response must be of finite duration due to restriction on available lengths of substrate material. A limit on the length of impulse response will cause a corresponding limit on the filter skirt response. In cases where a truncation of a given impulse response is necessary, a weighting function is usually used to ensure a gradual reduction of the response rather than an abrupt truncation which may cause serious ripple in the filter passband and high sidelobes in the stopband. The design of surface wave filters is discussed to some length by Hartmann et. al. [20] and Tancrell and Holland [25].

6.1 The unidirectional transducer

The common biphase interdigital transducer, having alternate fingers driven by electrical signals 180° out of phase, has the disadvantage of being bidirectional. Signals applied to one of these transducers will be launched equally in both the forward and reverse directions - this will result in a 3db transmission loss. By reciprocity there will also be 3db loss in receiving these signals. The resulting reflected signal gives rise to the triple transit response. Several unidirectional interdigital transducers have been developed. However, most have some undesirable feature, such as bandwidth limitation or fabrication complexity. The unidirectional transducer developed by Hartmann et. al. [60], appears to have none of the drawbacks of other unidirectional transducers, except for fabrication complexity. It is a three phase transducer having three electrode groups, each being driven by a signal which is 120° out of phase with the two other electrode signals (see figure 15). This transducer can provide a 20db or better front to back ratio over a 20% bandwidth and has been used in applications for low insertion loss delay lines providing a loss of the order of 1 - 2db.

6.2 The multistrip coupler

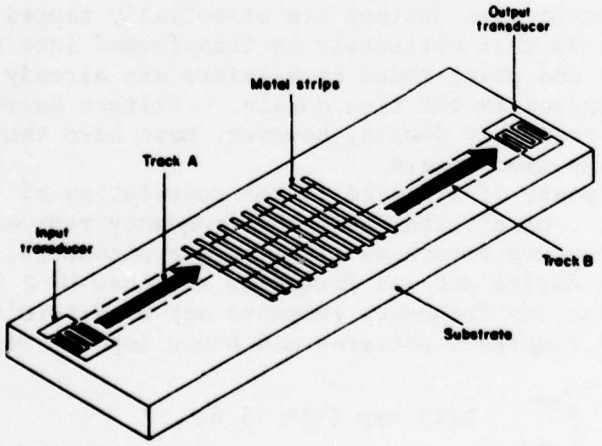

Figure 48. A multistrip coupler used as a track changer

The multistrip coupler shown in figure 48 is a broadband directional coupler which may be used to transfer surface acoustic wave energy from one acoustic path to another acoustic path with low loss. Multistrip couplers may be used for 'magic Ts', unidirectional transducers, surface wave mirrors with very low reflection loss, reduction of bulk wave responses and many other applications. One application of great significance is in the field of surface wave filters. In general, if one transducer, either the launch or receiving transducer, is apodized,

then the other transducer must be unapodized. This is because the wave front of an apodized transducer is not uniform in amplitude. A multistrip coupler placed between the launch and receive transducer, now on different tracks, will average the wave front from the launch transducer causing a uniform wave front on the second transducer and allow both input and output transducers to be apodized. This means that for the case where the input and output transducers are identical, the frequency response will be the square of the Fourier transform of the impulse response of a single transducer. This will have the effect of doubling (in db) the stopband rejection and doubling the skirt steepness but not significantly changing the insertion loss. Also as the multistrip coupler causes the surface wave to change tracks but not so the bulk wave, then the bulk wave from the launch transducer will miss the receive transducer and thereby eliminate its spurious response. See Tancrell, [24], and Deacon et. al. [19]. The optimum length of a multistrip coupler is proportional to the inverse of the electro-mechanical coupling coefficient. Multistrip couplers on Lithium Niobate are quite small and efficient due to that material's high electro-mechanical coupling coefficient. Unfortunately, quartz has such a low electro-mechanical coupling coefficient that multistrip coupler lengths are impractical. The design and applications of multistrip couplers are discussed to some length by Marshall et. al. [63] and [64].

6.3 Transducer stripe to gap ratio

Transducer stripe to gap ratio determines the electric field distribution in the surface wave substrate and hence the degree of excitation of the fundamental and harmonic surface waves. It also determines the degree of reflection caused by the metal electrodes short circuiting the electric field, see figure 17. An analysis of the excitation of surface waves at harmonics of the transducer fundamental frequency for the conventional and split finger transducer configurations has been carried out by Smith [66]. Results for the conventional single finger geometry are illustrated in figure 49 where surface wave excitation as a function of metallization ratio is shown for harmonics up to the eleventh. Similar results are given for the split finger geometry in figure 50.

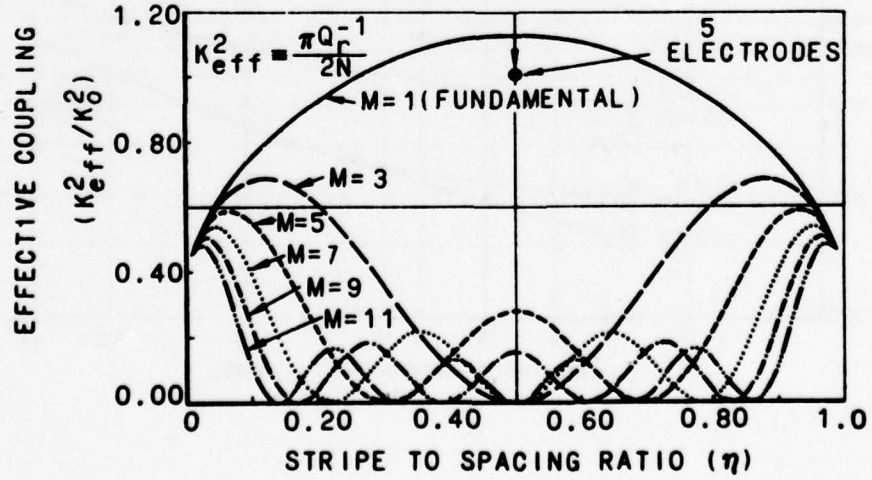

Figure 49. Harmonic excitation for conventional λ/4 transducer electrodes as a function of metallization ratio [66]

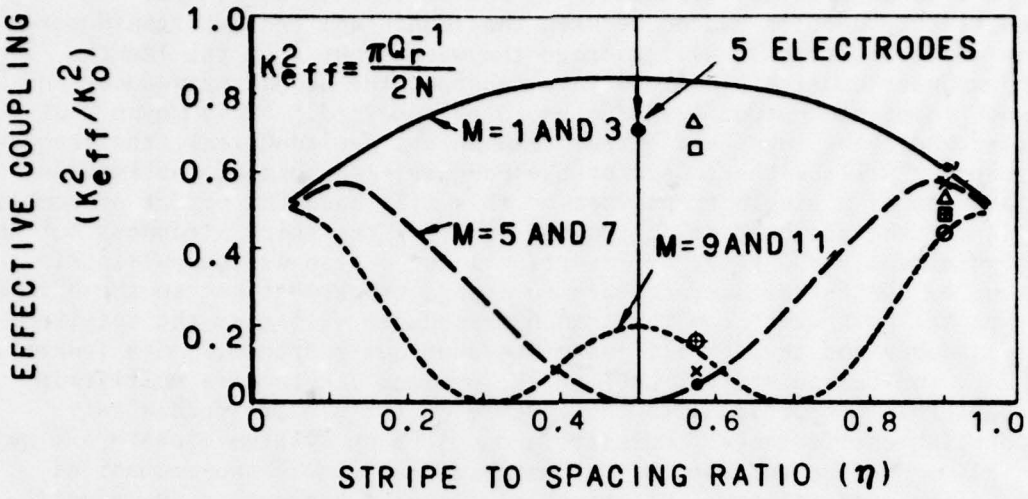

Figure 50. Effective coupling coefficient (k^2) for harmonic excitation of split finger electrodes as a function of metallisation ratio [66]

Hickernell et. al. [40] have empirically determined the electrical discharge breakdown voltage between adjacent interdigital transducer electrodes as a function of electrode gap. These results shown in figure 51 indicate that for the majority of appplications electrical breakdown will not be a problem.

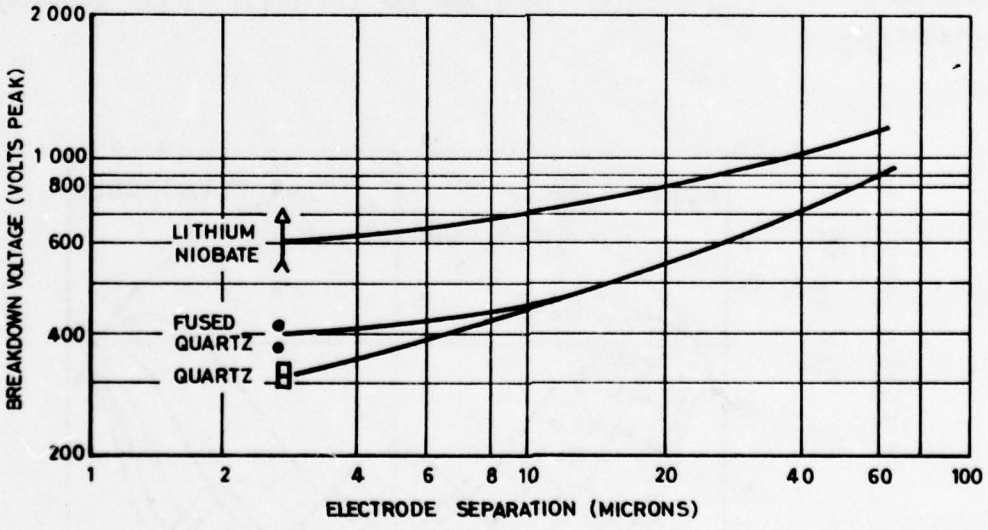

Figure 51. Pulsed d.c. voltage breakdown in air between interdigital electrodes (atmospheric pressure)[40]

6.4 Transducer beamwidth

The main factors determining the required transducer beamwidth are the loss due to beam steering and diffraction and the desired transducer radiation immittance. If transducers are made too wide, then each finger will have a significant resistive loss. Typical transducer widths are of the order of 50 to a few 100 wavelengths. Note that for a given substrate material, the radiation admittance is proportional to the transducer width and the number of periodic sections squared.

Larkin [43], has derived expressions for transducer efficiency as a function of transducer aperture and sheet resistivity for both ST Quartz and Lithium Niobate. These results are shown plotted in figure 52. Maerfeld et. al. [45], have carried out a similar analysis of the resistive losses in multistrip couplers.

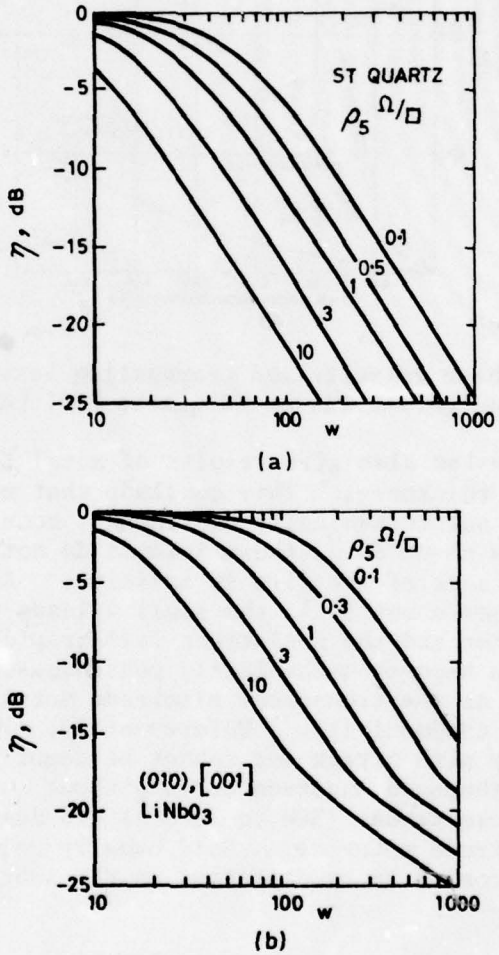

Figure 52. Electrode efficiency in decibels as a function of aperture [43]

6.5 Transducer electrode metallisation

To determine the thickness of transducer metal electrodes, the designer must trade off electrode resistance with the mass loading of the electrode on the substrate surface. Figure 53 illustrates the effects of metal film thickness on surface wave velocity and attenuation for both Gold and Aluminium on a Quartz substrate. This figure combines the results of Pouliquen and Vaesken [46], and Combon and Rouzeyre [39].

Values of attenuation (db/cm) may be linearly interpolated for frequencies other than those shown.

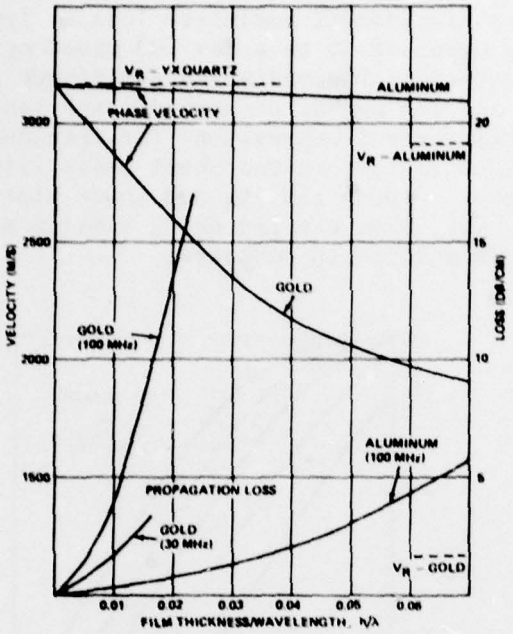

Figure 53. Phase velocity and propagation loss for aluminium and gold films on YX quartz [39] [46]

Pouliquen and Vaesken also give results of metal film resistance as a function of film thickness. They conclude that metal films below about 500 to 600 Å are not mechanically continuous, consisting of small islands of atoms. Below about 50 Å, these islands do not touch and the electrical resistance of the film is infinite. As the metal film thickness increases about 50 Å, the small islands of metal atoms begin to contact one another and the resistance falls rapidly until at about 500 to 600 Å the film becomes mechanically continuous. Aluminium has been used extensively as the transducer electrode metal because of its low mass density and high conductivity. Unfortunately, Aluminium has a great chemical affinity with oxygen and cannot be deposited in thicknesses of less than a few thousand Angstrom units without quickly oxidising. If very thin metal electrodes (500 to 1000 Å) are desired, then Gold may be used as the electrode material. Gold usually requires a keying layer of about 50 Å of Chromium to be deposited on the substrate to aid bonding.

7. PRACTICAL RESULTS

Several SAW devices have been designed and fabricated at the Defence Research Centre Salisbury, using the principles discussed in this paper. At this stage there is insufficient time to include a complete analysis of any particular device; however brief results from two of the devices will be given here.

7.1 Phase coded sequence generator/correlator

The first devices fabricated were a pair of phase coded sequence generator/correlators similar to the one discussed in paragraph 3.2. They have a centre frequency of 70 Mlz and a chip or phase reversal rate of 10 Mlz with 127 phase coded taps. The devices were fabricated

on ST quartz because of its stable temperature coefficient. $\lambda/4$ fingers were used and the finger and gap width were both 11.28×10^{-6} m, with finger overlap being about 150 λ. Gold metallization of 750 Å thickness was used, however, from experience gained since that time better results would have been achieved by using 2000 to 3000 Å of Aluminium.

Figures 54 and 55 illustrate the result obtained when using the device as a code generator. Figure 54 shows the output of the phase coded array when an electrical impulse is applied to one of the end transducers, and figure 55 is an expanded version of figure 54 showing the details of the phase reversals.

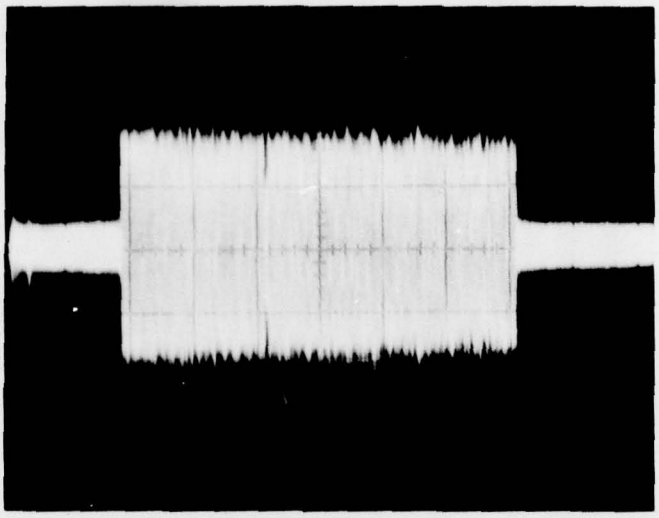

2 μs/div

Figure 54. Phase coded array response to an electrical impulse

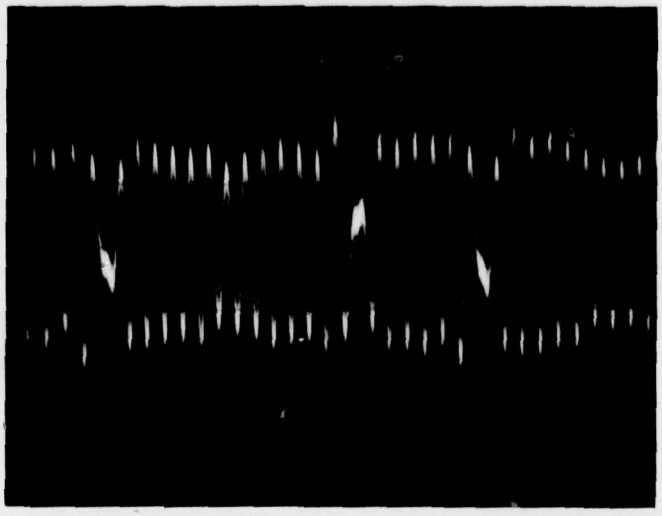

50 ns/div

Figure 55. Expanded impulse response of phase coded array

Figures 56 and 57 show the results when the second device is used to correlate the waveform of the first device. Figure 56 shows the correlation peaks standing out clearly from the cross correlation noise. Figure 57 is an expansion of the cross correlation peak showing the almost ideal triangular shape. The cross correlation noise is considerably worse than predicted from theory; this is caused largely by the two devices being made at separate times with separate photographic masters, resulting in slightly different centre frequencies.

Figure 56. Response of phase coded array to its matching waveform

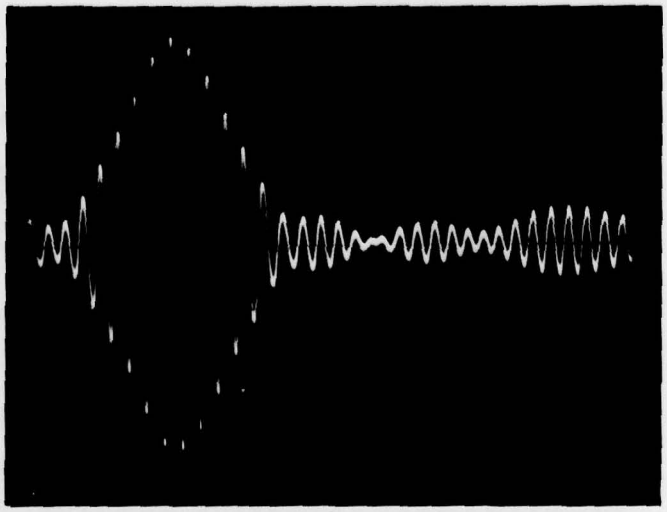

50 ns/div

Figure 57. Correlation peak of phase coded array

7.2 150 MHz bandpass filter

A bandpass filter having 150 mHz centre frequency with a bandwidth of 10 MHz was fabricated. This device, shown in figure 58 has two transducers which have been weighted in a sin x/x pattern and coupled together by a multistrip coupler. The $\lambda/8$ split finger configuration has been used giving the end transducer finger and gap widths of 2.85×10^{-6}m. The aperture or finger overlap is about 60λ. The multistrip coupler has 110 strips each of 4.28×10^{-6}m wide. Aluminium metallization of 2000 Å thickness has been used and Lithium Niobate was chosen as the substrate material because of its high coupling coefficient. Insertion loss for this device is about 13db. Figure 59 shows the filter response.

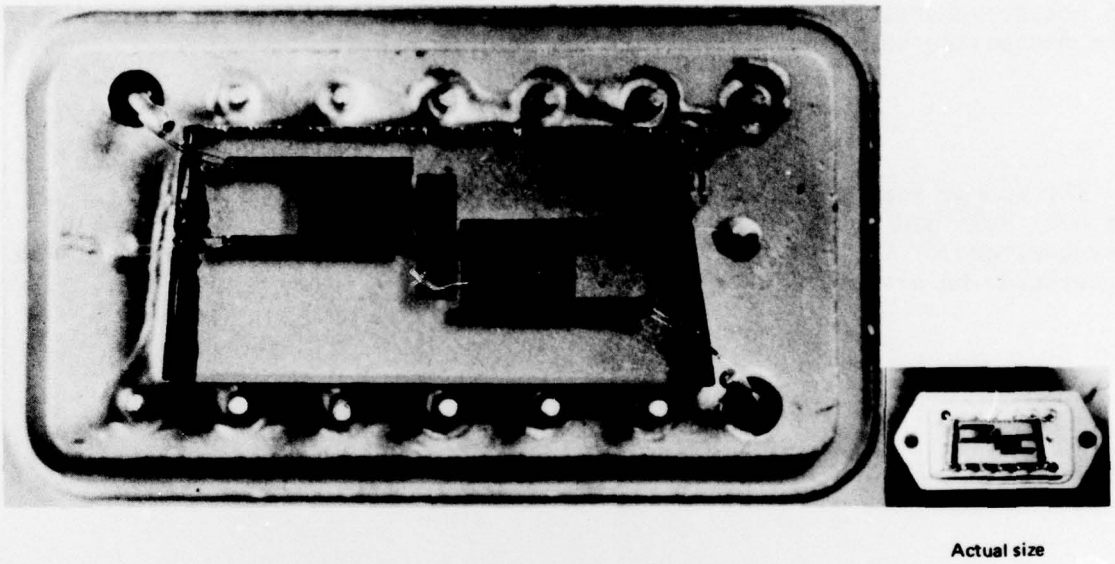

Figure 58. 150 MHz filter

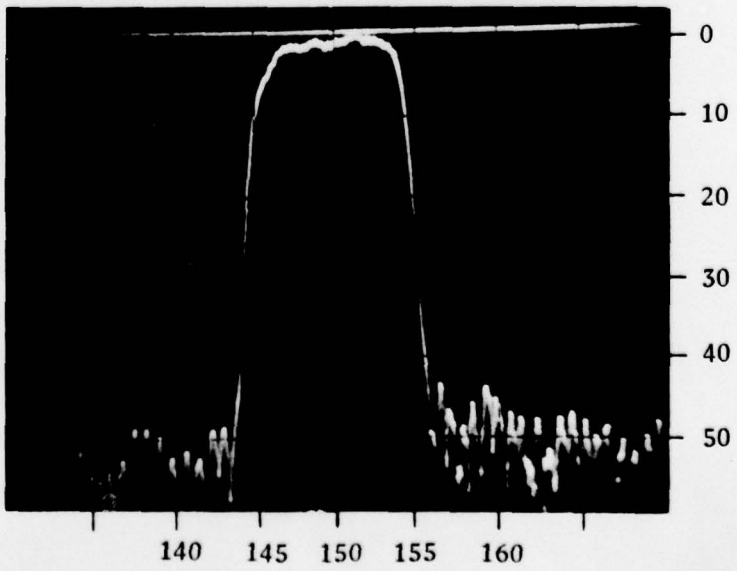

Figure 59. 150 MHz filter frequency response

8. CONCLUSIONS

The fundamental properties of SAW devices have been reviewed and the practical design considerations have been discussed, with several devices having been successfully designed and fabricated using the principles outlined in this paper.

Although SAW technology is still a developing technology, it has reached a level of maturity where many useful devices can be readily designed and fabricated by a photo lithographic process which lends itself to mass production. Matched filters, bandpass filters and oscillators all fit into this category and all exhibit superior performance at greatly reduced sizes when compared with their conventional couterparts.

Over the next decade it is expected that many new devices will be developed and that many improvements will be made to existing devices by the development of better substrates, new transducer geometries and a better understanding of the mechanisms which now degrade device performance.

9. ACKNOWLEDGEMENT

The author gratefully acknowledges the enthusiastic support of Mr D.W. Neal and staff of Micro-Engineering Group who fabricated the SAW devices, and of Computer Aided Processes Group and Drawing Office staff who generated the artwork.

REFERENCES

No.	Author	Title
General Overviews		
1	Farnell, G.W. and Adler, E.L.	"An Overview of Acoustic Surface Wave Technology" Dept. of Electrical Engineering, McGill University. Final Report to Communications Research Centre on DSS Contract 36001-3-4406, August 1974.
2	Holland, M.G. and Claiborne, L.T.	"Practical Surface Acoustic Wave Devices" Proc. IEEE, Vol. 62, No. 5, May 1974.
3	Maines, J.D. and Paige, E.C.S.	"Surface-Acoustic-Wave Components Devices and Applications" Proc. IEE, Vol. 120, No. 10R, October 1973.
SAW Fundamentals		
4	deKlerk, J.	"Ultrasonic Transducers, 3. Surface Wave Transducers". Ultrasonics, January 1971.
5	White, R.M.	"Surface Elastic Waves" Proc. IEEE, Vol. 58, No. 8, August 1970.
6	White, R.M. and Voltmer, F.W.	"Direct Piezo-electric Coupling to Surface Elastic Waves". Applied Physics Letters, Vol. 7, No. 12, 15th December 1965.
Chirp Filters		
7	Gerard, H.M., Smith, W.R., Jones, W.R. and Harrington, J.B.	"The Design and Application of Highly Dispersive Acoustic Surface-Wave Filters", IEEE Trans. on Microwave Theory and Techniques, Vol. MTT-21, No. 4, April 1973.
8	Heighway, J. and Deacon, J.M.	"A Continuous Phase Analysis of Dispersive S.A.W. Transducers", Proc. 1972, IEEE Ultrasonics Symposium (Boston, Massachusetts, October 1972).
9	Jones, W.S., Kempf, R.A., and Hartmann, C.S.	"Practical Surface Wave Chirp Filters for Modern Radar Systems", Microwave Journal, May 1972.

No.	Author	Title
10	Maines, J.D., and Johnston, J.N.	"Surface Acoustic Wave Devices and Applications. 2. Pulse Compression Systems", Ultrasonics, September 1973.
11	Morgan, D.P.	"Log-Periodic Transducers for Acoustic Surface Waves" Proc. IEE, Vol. 119, No. 1, January 1972.
12	Tancrell, R.H. and Holland, M.G.	"Acoustic Surface Wave Filters", Proc. IEEE, Vol. 59, No. 3, March 1971.
Phase Coded Devices		
13	Bell, D.T. Jr., Holmes, J.D. and Ridings, R.V.	"Application of Acoustic Surface-Wave Technology to Spread Spectrum Communications", IEEE Trans. Microwave Theory and Techniques, Vol. MTT-21, No. 4, April 1973.
14	Carr, P.H., De Vito, P., and Szabo, T.L.	"The Effect of Temperature and Doppler Shift on the Performance of Elastic Surface Wave Encoders and Decoders". IEEE Trans. Sonics and Ultrasonics, Vol. SU-19, 1972, 357-367.
15	Hunsinger, B.J. and Franck, A.R.	"Programmable Surface-Wave Tapped Delay Line". IEEE Trans. Sonics and Ultrasonics, Vol. SU-18, No. 3, July 1971.
16	Jones, W.S., Hartmann, C.S., and Claiborne, L.T.	"Evaluation of Digitally Coded Acoustic Surface-Wave Matched Filters". IEEE Trans. Sonics and Ultrasonics, Vol. SU-18, No. 1, January 1971.
17	Lever, K.V., Patterson, E., and Wilson, I.M.	"Analysis of Effect of Fabrication Errors on Performance of Surface-Acoustic-Wave M-Sequence Correlators", Proc. IEE, Vol. 122, No. 12, December 1975.
18	Staples, E.J. and Claiborne, L.T.	"A Review of Device Technology for Programmable Surface-Wave Filters". IEEE Trans. Microwave Theory and Techniques, Vol. MTT-21, No. 4, April 1973.

No.	Author	Title
Bandpass Filters		
19	Deacon, J.M., Heighway, J., and Jenkins, J.A.	"Multistrip Coupler in Acoustic Surface-Wave Filters". Electronics Letters 17th May, 1973, Vol. 9, No. 10.
20	Hartmann, C.S., Bell, D.T., and Rosenfeld, R.C.	"Impulse Model Design of Acoustic Surface-Wave Filters". IEEE Trans. Microwave Theory and Techniques, Vol. MTT-21, No. 4, April 1973.
21	McClellan, J.H., Parks, T.W., and Rabiner, L.R.	"A Computer Program for Designing Optimum FIR Linear Phase Digital Filters". IEEE Trans. Audio and Electro-acoustics, Vol. AU-21, No. 6, December 1973.
22	Matthaei, G.L.	"Acoustic Surface-Wave Transversal Filters". IEEE Trans. Circuit Theory, Vol. CT-20, No. 5, September 1973.
23	Tancrell, R.H.	"Analytic Design of Surface Wave Bandpass Filters". IEEE Trans. Sonics and Ultrasonics, Vol. SU-21, No. 1, January 1974.
24	Tancrell, R.H.	"Improvement of an Acoustic Surface-Wave Filter with a Multistrip Coupler". Electronics Letters, 12th July 1973, Vol. 9, No. 14.
25	Tancrell, R.H. and Holland, M.G.	"Acoustic Surface-Wave Filters", Proc. IEEE Vol. 59, No. 3, March 1971.
Oscillators		
26	Bale, R. and Lewis, M.F.	"Improvements to the SAW Oscillator". Proc. 1974, IEEE Ultrasonics Symposium, (Milwaukee, WI 1974) PP272-275.
27	Crabb, J., Lewis, M.F. and Maines, J.D.	"Surface Acoustic-Wave Oscillators: Mode Selection and Frequency Modulation", Electronics Letters, 9, No. 10, May 1973.
28	Davies, L.W. and Lawrence, M.W.	"Prospects for Surface Elastic Wave Crystal-controlled Delay Line Oscillators", Proc. I.R.E.E. Australia, February 1971.

29 Lawrence, M.W. "Surface-Elastic-Wave Delay Line Oscillators". AWA Technical Review, Vol. 15, No. 2, 1973.

30 Lewis, M.F. "Surface-Acoustic-Wave Devices and Applications. 6. Oscillators - The Next Successful Surface-Acoustic-Wave Device?". Ultrasonics. May 1974.

Synthesisers

31 Browning, I., Crabb, J. and Lewis, M.F. "A SAW Frequency Synthesiser". Proc. 1975, IEEE Ultrasonics Symposium, IEEE Cat. No. CHO-994-4SU.

32 Budreau, A.J., Carr, P.H., and Laker, K.R. "Frequency Synthesizer Using Acoustic-Surface-Wave Filters". Microwave Journal, March 1974.

Convolvers

33 Kino, G.S., Ludvik, S., Shaw, H.J. Shreve, W.R., White, J.M., and Winshaw, D.K. "Signal Processing by Parametric Interactions in Delay-Line Devices". IEEE Trans. Microwave Theory and Techniques, Vol. MTT-21, No. 4, April 1973.

34 Luukkala, M., and Kino, G.S. "Convolution and Time Inversion using Parametric Interactions of Acoustic-Surface-Waves. Applied Physics Letters, Vol. 18, No. 9, 1st May 1971.

35 Nudd, G.R., and Otto, O.W. "Real-Time Fourier Analysis of Spread Spectrum Signals Using Surface-Wave-Implemented Chirp-Z Transformation". IEEE Trans. Microwave Theory and Techniques. January 1976.

36 Otto, O.W. "Real Time Fourier Transform with a Surface-Wave Convolver". Electronics Letters 14th December 1972, Vol. 8, No. 25.

37 Otto, O.W. and Moll, N.J. "Lithium-Niobate-Silicon Surface-Wave Convolver". Electronics Letters 30th November 1972, Vol. 8, No. 24.

No.	Author	Title
Second Order Effects		
38	Bristol, T.W., Jones, W.R., Snow, P.B. and Smith, W.R.	"Applications of Double Electrodes in Acoustic Surface-Wave Device Design". Proc. 1972 IEEE Ultrasonics Symposium (Boston Massachusetts, October 1972) 72-CHO 708-8SU.
39	Cambon, G., and Rouzeyre, M.	"Attenuation of Dispersive Rayleigh Waves on Quartz". Electronics Letters, Vol. 6, No. 17, 20th August 1970.
40	Hickernell, F.S., Clar, P.L., and Cook, I.R.	"Pulsed D.C. Voltage Breakdown Between Interdigital Electrodes" Proc. 1972 Ultrasonics Symposium (Boston Massachusetts October 1972) 72 CHO 708-8SU.
41	Jones, W.S., Hartmann, C.S., Sturdivant, T.D.	"Second Order Effects in Surface Wave Devices". IEEE Trans. Sonics and Ultrasonics, Vol. SU-19, No. 3, July 1972.
42	Judd, G.W., Jones, W.R. and Bristol, T.W.	"An Improved Tapping Transducer Geometry for Surface Wave Phase Coded Delay Lines", Proc. 1972 IEEE Ultrasonics Symposium (Boston, Massachusetts, October 1972) 72 CHO 708-8SU.
43	Larkin, K.M.	"Electrode Resistance Effects in Interdigital Transducers". IEEE Trans. Microwave Theory and Techniques, Vol. MIT-22, No. 4, April 1974.
44	LaRose, R. and Vasile, C.F.	"Broadband Bulk-Wave Cancellation in Acoustic Surface-Wave Devices", Electronics Letters, Vol. 8, No. 19, 21st September 1972.
45	Maerfeld, C., Gordon, K. and Farnell, C.W.	"Resistive Losses in Acoustic Surface-Wave Multistrip Couplers", IEEE Trans. on Sonics and Ultrasonics, Vol. SU-22, No. 5, September 1975.
46	Pouliquen, J. and Vaesken, G.	"Effect of a Metallic Thin Film on the Propagation of Rayleigh Waves", Journal of Applied Physics, Vol. 44, No. 4, April 1973.
47	Ristic, V.M.	"Bulk Mode Generation in Surface-Wave Devices". Proc. 1972 IEEE Ultrasonics Symposium (Boston, Massachusetts, October 1972), 72CHO 708-8SU.

No.	Author	Title
48	Schulz, M.B. and Holland, M.G.	"Surface Acoustic Wave Delay Lines with Small Temperature Coefficient" Proc. IEEE. September 1970.
49	Skeie, H.	"Mechanical and Electrical Reflections in Interdigital Transducers". Proc. 1972, IEEE Ultrasonics Symposium (Boston Massachusetts, October 1972) 72 CHO 708-8SU.
50	Slobodnik, A.J.	"A Review of Material Trade-Offs in the Design of Acoustic Surface Wave Devices at VHF and Microwave Frequencies". IEEE Trans. Sonics and Ultrasonics. Vol. SU-20, No. 4, October 1973.
51	Szabo, T.L. and Slobodnik, A.J.	"Acoustic Surface Wave Diffraction and Beamsteering". Air Force Cambridge Research Laboratories Publication, AFCRL-TR-73-0302, 3rd May 1973, Physical Sciences Research Paper No. 548.
52	Tancrell, R.H. and Meyer, P.C.	"Operation of Long Surface Wave Interdigital Transducers". 1971 IEEE Ultrasonics Symposium, Miami, Florida, December 1971.
53	Tancrell, R.H. and Williamson, R.C.	"Wavefront Distortion of Acoustic Surface Waves from Apodized Interdigital Transducers", Applied Physics Letters, Vol. 19, No. 11, 1st December 1971.
54	Tanski, W., Acevedo, J. and Moore, R.A.	"A Bulk Mode Suppression Technique for Surface Wave Devices", Proc. IEEE, 1973 Ultrasonics Symposium, (Monterey, California).

Transducer Analysis

55	Bristol, T.W.	"Analysis and Design of Surface Acoustic Wave Transducers", IEE Conference on Component Performance and Systems Applications of Surface Acoustic Wave Devices, Aviemore, Scotland, IEE Conference Publication No. 109.

No.	Author	Title
56	Emtage, P.R.	"Self Consistent Theory of Interdigital Transducers", Proc. 1972 IEEE Ultrasonics Symposium (Boston, Massachusetts, October 1972) 72 CHO 708-8SU.
57	Engan, H.	"Excitation of Elastic Surface Waves by Spatial Harmonics of Interdigital Transducers" IEEE Trans. on Electron Devices, Vol. ED16, No. 12, December 1969.
58	Farnell, G.W., Cermak, I.A., Silvester, P, and Wong, S.K.	"Capacitance and Field Distributions for Interdigital Surface-Wave Transducers" IEEE Trans. on Sonics and Ultrasonics, Vol. SU-17, No. 3, July 1970.
59	Gerard, H.M.	"Acoustic Scattering Parameters of the Electrically Loaded Interdigital Surface Wave Transducer", IEEE Trans. Microwave Theory and Techniques, Vol. MTT-17, No. 11, November 1969.
60	Hartmann, C.S., Jones, W.S., and Vollers, H.	"Wideband Unidirectional Surface Wave Transducers", IEEE Trans. on Sonics and Ultrasonics Vol. SU-19, No. 3, July 1972.
61	Heighway, J., Tarant, D.W., and Oxley, C.H.	"Simple Approach to the Design of Interface Networks for Acoustic Surface-Wave Filters", Electronics Letters, Vol. 8, No. 26, 28th December 1972.
62	Ingebrigtsen, K.A.	"Analysis of Interdigital Transducers". Proc. 1972 Ultrasonics Symposiums (Boston, Massachusetts, October 1972), 72 CHO 708-8SU.
63	Marshall, F.G., Newton, C.O., and Paige, E.G.S.	"Theory and Design of the Surface Acoustic Wave Multistrip Coupler" IEEE Trans. on Microwave Theory and Techniques Vol. MTT-21, No. 4, April 1973.
64	Marshall, F.G., Newton, C.O., and Paige, E.G.S.	"Surface Acoustic Wave Multistrip Components and their Applications", IEEE Transactions on Microwave Theory and Techniques, Vol. MTT-21, No. 4, April 1973.

No.	Author	Title
65	Milsom, R.F. and Redwood, M.	"Interdigital Piezo-electric Rayleigh Wave Transducer: An Improved Equivalent Circuit", Electronics Letters, Vol. 7, No. 9, 6th May 1971.
66	Smith, W.R.	"Circuit Model Analysis for Interdigital Transducers with Arbitrary Stripe-to-Gap Ratios, Polarity Sequences and Harmonic Operation" Proc. 1974, IEEE Ultrasonics Symposium (Milwaukee, Wisonsin, November 1974) 74 CHO 896-1SU.
67	Smith, W.R., Gerard, H.M. and Jones, W.R.	"Analysis and Design of Dispersive Interdigital Surface-Wave Transducers", IEEE Trans. Microwave Theory Tech., MTT-20, (1972), 458-471.
68	Smith, W.R., Gerard, H.M., Collins, J.H., Reeder, T.M., and Shaw, H.J.	"Analysis of Interdigital Surface Wave Transducers by Use of an Equivalent Circuit Model" IEEE Trans. on Microwave Theory and Technique, Vol. MTT-17, No. 11, November 1969.
69	Smith, W.R., Gerard, H.M., Collins, J.H., Reeder, T.M., and Shaw, H.J.	"Design of Surface Wave Delay Lines with Interdigital Transducers", IEEE Trans. on Microwave Theory and Techniques, Vol. MTT-17, No. 11, November 1969.

DISTRIBUTION

	Copy No.
EXTERNAL	
In United Kingdom	
Defence Scientific and Technical Representative, London	1
In United States of America	
Counsellor, Defence Science, Washington	2
In Australia	
Chief Defence Scientist	3
Army Scientific Adviser	4
Navy Scientific Adviser	5
Air Force Scientific Adviser	6
Executive Controller (Australian Defence Scientific Service)	7
Superintendent (Defence Science Administration)	8
Defence Information Services Branch (for microfilming)	9
Defence Information Services Branch for:	
United Kingdom, Ministry of Defence, Defence Research Information Centre (DRIC)	10
United States, Department of Defense,	11 - 22
Canada, Department of National Defence, Defence Science Information Service	23
New Zealand, Department of Defence	24
Australian National Library (Through STIB)	25
Defence Library, Campbell Park	26
Library, Aeronautical Research Laboratories	27
Library, Materials Research Laboratories	28
Director, Joint Intelligence Organisation (DDSTI)	29
WITHIN DRCS	
Chairman, Defence Research Centre Salisbury Management Committee	30
Chief Superintendent, Advanced Engineering Laboratory	31
Superintendent, Communications and Electronic Engineering Division	32
Superintendent, Workshops and Mechanical Design Division	33
Superintendent, Systems Analysis Division	34
Superintendent, Electronics Division	35
Superintendent, Weapon Systems Division	36
Senior Principal Research Scientist, Electronic Warfare	37
Senior Principal Research Scientist, Radar Technology	38

	Copy No.
Principal Engineer, Communications	39
Principal Officer, Communications Technology Group	40
Principal Officer, Radar and Electronic Tracking Group	41
Principal Officer, Radio Group	42
Principal Officer, Electronic Warfare Development Group	43
Principal Officer, Micro-Engineering Group	44
Principal Officer, Tropospheric Studies Group	45
Principal Officer, Systems Development Group	46
Principal Officer, Ionospheric Studies Group	47
Principal Officer, Tracking and Command Systems Group	48
Principal Officer, Telecommunications Engineering Group	49
Dr A.S. Burgess, Underwater Detection Group	50
Mr D. Neal, Micro-Engineering Group	51
Author	52 - 53
DOC Section CEE Division Headquarters	54
Library	55 - 56
Spares	57 - 62